Physics-based and Data-driven Modeling of Degradation Mechanisms for Lithium-Ion Batteries - A Review

Ruiz, Pedro Lozano; Damianakis, Nikolaos; Mouli, Gautham Ram Chandra

DOI
10.1109/ACCESS.2025.3535918

Publication date
2025

Document Version
Final published version

Published in
IEEE Access

IEEE Access
Multidisciplinary | Rapid Review | Open Access Journal

Received 18 November 2024, accepted 17 January 2025, date of publication 29 January 2025, date of current version 3 February 2025.

Digital Object Identifier 10.1109/ACCESS.2025.3535918

TOPICAL REVIEW

Physics-Based and Data-Driven Modeling of Degradation Mechanisms for Lithium-Ion Batteries–A Review

PEDRO LOZANO RUIZ[1], (Student Member, IEEE), NIKOLAOS DAMIANAKIS[2], (Graduate Student Member, IEEE), AND GAUTHAM RAM CHANDRA MOULI[2], (Member, IEEE)

[1]Department of Power Management, Sonova AG, 8712 Stäfa, Switzerland
[2]Department of Electrical Sustainable Energy, Delft University of Technology, 2628 CD Delft, The Netherlands

Corresponding author: Nikolaos Damianakis (N.Damianakis@tudelft.nl)

This work was supported by the Dutch Research Council (NWO) as part of the Ongoing Research Project "New Energy and Mobility Outlook for the Netherlands" (NEON) of the Research Program Crossover under Project 17628.

ABSTRACT Lithium-ion batteries (LIB) are widely used in various applications. The LIB degradation curve and, most significantly, the knee-point and End-of-life (EoL) point identification are critical factors for the selection of the appropriate application, such as electric vehicles and stationary energy storage systems, due to their effect on performance and lifespan, safety, and environmental footprint. Linear degradation models can be inaccurate in capturing the highly nonlinear behavior of LIB degradation caused by multiple simultaneous degradation mechanisms. Hence, this work first analyzes the main different mechanisms, their causes, and their interrelations. Secondly, the various single- and multi-mechanism physics-based (PB) and data-driven (DD) models for LIB degradation and knee-point identification are summarized and compared regarding their prediction performance on degradation and transition from stabilized to saturated aging. While single-mechanism PB models can be effective in the LIB first-life prediction, they can seriously undermine the knee-point and saturated aging. Moreover, the modeling of the different aging mechanisms can significantly increase the complexity of the multi-mechanism PB models. Finally, while DD models for LIB degradation have been developed, a DD model focused on knee-point identification and LIB second-life is still missing from the literature.

INDEX TERMS Lithium-ion batteries (LIB), degradation, degradation mechanisms, knee-point, physics-based, data-driven.

I. INTRODUCTION

A. GENERAL BACKGROUND

Lithium-ion batteries (LIBs) are the most widely used technology for energy storage in Electric Vehicles (EVs). Compared to other electrochemical storage devices, such as Ni-MH batteries, lead-acid batteries, or capacitors, LIBs provide the best trade-off between specific energy, specific power, and number of cycles [1]. Over their lifetime, LIBs lose capacity through two mechanisms: on the one hand, cells undergo calendar aging while being stored as a result of side reactions resulting from the thermodynamic instability of materials; on the other hand, repeatedly charging and discharging the cell induces kinetical effects such as volume variations or concentration gradients in a process known as cyclic aging [2]. The period during which LIBs are suitable for use in EVs is, therefore, limited. Beyond a certain point, their capacity and power fade so that they cannot guarantee a mileage per full charge above the necessary to avoid range anxiety. Typically, LIBs are retired from EV use when their capacity falls below 70% to 80% of the initial value [3]. This results in the useful life of LIBs being divided into two periods: First Life (FL) and Second Life (SL). To ensure the safe operation of the modules during the SL, the identification of the retirement point (End-of-life EoL) is key [4], [5].

The associate editor coordinating the review of this manuscript and approving it for publication was Branislav Hredzak.

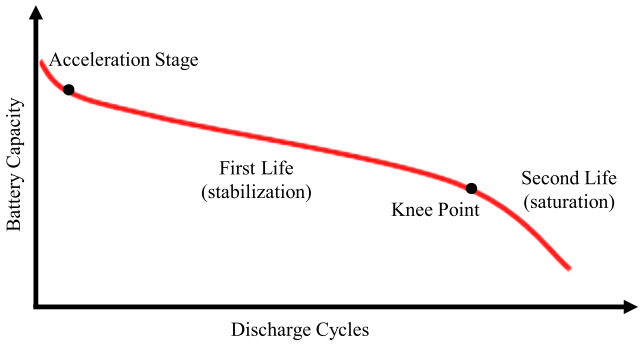

FIGURE 1. Battery Capacity Fade Timeline (First life, knee-point & Second life).

Once the FL is over, the battery may be reconditioned and used for a different purpose during its re-utilization stage. SL's possible applications include importing used LIBs into another EV or integrating them into the electrical grid as stationary storage. In [6], a life-cycle assessment was carried out on the environmental impact of these two applications, calculating the total carbon emissions in $kgCO_2eq/kWh$. It was found that re-utilization reduces the impact on climate change and acidification by 16% and 25%, respectively. Moreover, different stationary applications exist for SL battery integration in the power grid, such as residential demand response management and power smoothing for grid-scale photovoltaic plants [7].

Degradation causes and mechanisms of LIBs have been assessed several times in the literature [8], [9], [10], [11]. Each degradation mechanism is associated with one or more of the following degradation causes: time, C-rate, charge throughput, cut-off voltage, temperature, state-of-charge (SoC), and depth-of-discharge (DoD) [12]. In turn, each degradation mechanism leads to one or more of the following aging modes: Loss of Lithium Inventory (LLI), Loss of Active Material (LAM), and Conductivity Loss (CL). Cell capacity decreases due to LLI and LAM, while cell power fades as a consequence of LAM and CL [12].

Although all aging modes take place throughout the entire life of LIBs, their event rates differ depending on the stage of their lifespan and the operating and storage conditions the cells are subjected to. In [10], a distinction is made between the degradation trends at different stages: during the first few cycles, solid electrolyte interface (SEI) formation at the anode surface leads to LLI and LAM, resulting in a fast decrease of capacity. Subsequently, capacity fades in a stabilized fashion during most of the battery life. As Figure 1 depicts, a slow and stabilized capacity degradation can be observed in LIBs up to a knee-point (FL), after which capacity fades rapidly (SL) until the cell's EoL [13]. When the knee-point is reached, other degradation mechanisms, such as lithium plating (LP), which provokes lithium deposition on the anode, become more relevant. Lithium plating leads to:

1) A more prominent drop in the capacity of the cell: a direct impact due to LLI.
2) An increase in the number of side reactions involving the electrolyte and the disuse of part of the anode surface for intercalation due to LAM.

Low temperatures, high cycling rates, poor cell balance, charging at very low or high SOC, and geometric misfits are factors that enhance lithium plating on the anode surface [9]. On top of that, transition metal dissolution (TMD), binder failures, and volume changes due to cyclic aging and SEI cracking negatively affect CL, leading to the appearance of the knee-point, after which the Internal Resistance (IR) increase is accelerated until the EoL is reached [14]. The calendar and cyclic stress factors applied on a LIB before reaching its aging knee determine the transition from stabilized to rapid degradation. These stress factors are sometimes interrelated and may be aggravated or alleviated depending on the chemistry of the cell.

Despite graphite and lithium metal being the focus of the vast majority of studies on anode aging, Li metal anodes are generally avoided in consumer cells as they suppose a potential safety hazard due to the increased risk of dendrites formation [15], [16]. The main cathode chemistries investigated in the literature are lithium-iron-phosphate (LFP) [17], [18], [19], [20], [21], [22], lithium-manganese-nickel-cobalt (NMC) [23], [24], [25], [26], [27], [28], and lithium-cobalt-oxide (LCO) [29], [30], [31], [32], [33], [34]. Chemistries such as lithium-manganese-oxide (LMO) [29], [30], [33], [35] and lithium-nickel-cobalt-aluminium-oxide (NCA) [34], [36], [37], [38] have also been investigated to a lower extent.

B. CONTRIBUTIONS AND WORK STRUCTURE

As Table 1 depicts, while reviews about LIB aging are present in the literature, most of them focused on degradation mechanisms (DM) and their stress factors; however, several of them analyzed only one DM, e.g. transition metal dissolution (TMD), neglecting to assess the interactions between the different mechanisms such as [39], [40], [41]. Moreover, LIB degradation has been modeled mainly with two big model families, physics-based (PB) models and data-driven (DD) models. Several studies focused on the review of only PB models [11] or DD models [43], unable to provide insights via a comprehensive comparison between them. Only the authors in [42] & [12] incorporated both analysis of DM, stress factors, and DM interactions as well as assessment and comparison of PB & DD LIB degradation approaches; however, only concerning lithium-plating and EV applications, respectively. Finally, a review of knee-point identification models is still missing from the literature. In this regard, the study's main contributions can be summarized as follows:

- This work analyzes the key different LIB degradation mechanisms, stress factors, and interactions responsible for the nonlinear nature of the degradation curve and knee-point appearance, summarizing the respective

TABLE 1. Contributions of existing literature review works about LIB degradation.

Works	Contributions					
	Degradation Mechanisms (DMs) & Stress Factors	DM Interrelations	Knee-point Models	Physics-based (PB) Models	Data-driven (DD) Models	PB-DD Comparison
[39]	✓ (for TMD)					
[40]	✓ (for SEI)			✓ (for SEI)		
[41]	✓ (for LP)			✓ (for LP)		
[23]	✓ (for NMCs)	✓ (for NMCs)		✓ (for NMCs)		
[42]	✓ (for LP)			✓ (for LP)	✓ (for LP)	✓ (for LP)
[10]	✓	✓				
[43]	✓	✓			✓ (semi-)empirical	
[11]	✓	✓		✓		
[44]	✓	✓			✓	
[45]				✓ (Calendar)	✓ (Calendar)	✓ (Calendar)
[12]	✓	✓		✓ (for EVs)	✓ (for EVs)	✓ (for EVs)
This Work	✓	✓	✓	✓	✓	✓

developed degradation and knee-point identification models that have not yet been thoroughly investigated.

- This work provides a comprehensive review of the two main degradation method families and their differences, the single- and multi-mechanism physics-based and data-driven modeling approaches, evaluating their completeness and accuracy for LIB degradation and knee-point prediction, which is still missing from the existing literature.

The authors believe that this work can provide valuable insights into the accuracy of the prediction of LIBs' FL, SL, and knee-point by the various existing models. Nowadays, this is critical for the proper use of the LIB in different applications (e.g. use as mobility or stationary energy storage) depending on the capacity fade curve due to safety and environmental reasons. It must be noted that, in this work, the anode and cathode denote the negative and positive electrodes, respectively, and these terms are used interchangeably. Moreover, this also applies to the use of the terms "degradation" and "aging." Finally, this work focused mostly on the capacity fade effect for the LIB degradation, rather than the power fade, since capacity fade is considered as the main factor for the proper application selection and re-utilization of LIBs [3].

This study is structured as follows: Section II provides a full overview of the most relevant degradation mechanisms, as well as a classification of the most significant stress variables impacting each mechanism. Section III offers an explanation of the knee-point as well as various analytical and numerical ways to calculate it. Section IV comprises a comparison of cutting-edge degradation modeling methodologies. This part covers three different modeling approaches: single- and multi-mechanism physics-based approaches in Section IV-A and Section IV-B respectively, and data-driven approaches in Section IV-C. Finally, Section V concludes the work.

II. DEGRADATION MECHANISMS IN LIBs AND NONLINEAR INTERACTION

As already explained in Section I, LIBs deteriorate as a result of a complex interplay of different physical and chemical mechanisms. Their rate of occurrence is determined by the different stress factors, along with the chemistry of the cell. From the moment a cell is charged for the first time, all degradation mechanisms are activated to different degrees. Among them, SEI formation is generally accepted as the most dominant mechanism in most situations [17], [47], [48]. Yet, after prolonged cycling, Li plating becomes more relevant based on the large amounts of metallic lithium at the anode surface detected in aged cells [2], [18], [49]. Moreover, other aging mechanisms are the mechanical stress on electrode materials [50], [51], [52], [53] and transition metal dissolution from the cathode and deposition in the anode [54], [55], [56], [57], [58]. This section analyses the above aging mechanisms, their causes, and influencing factors, and the conclusions reached in this regard. The effect on capacity fading of other mechanisms, such as formation and growth of cathode surface layer, are not included in the present study as they are assumed comparatively negligible [56], [59], [60].

A. SEI FORMATION AND GROWTH

1) DEFINITION & CAUSES

Electrolytes serve as the medium for the transfer of ions between the negative and the positive electrodes [62]. Their stability window is defined as the energy difference between the Highest Occupied Molecular Orbital (HOMO)

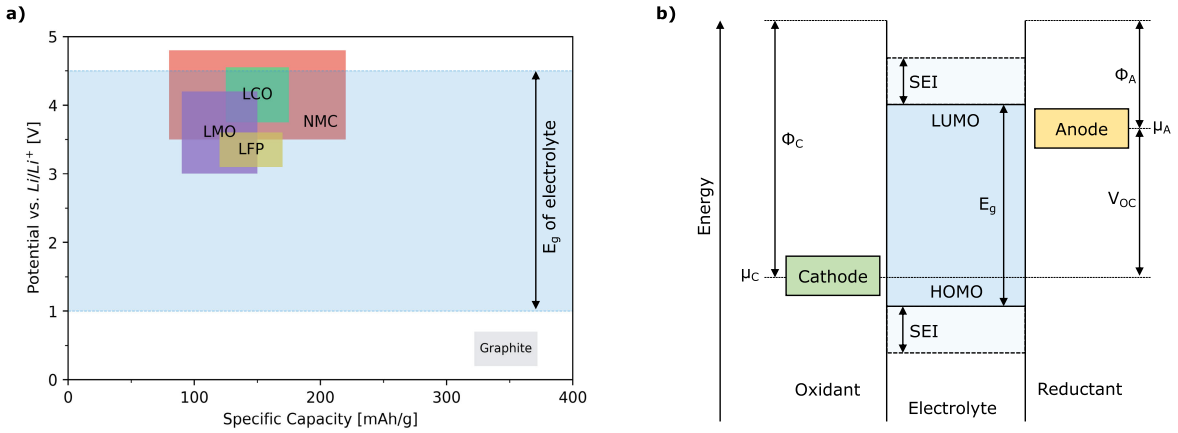

FIGURE 2. a) Potential versus specific capacity of some common electrode materials relative to the electrochemical stability window (E_g) of a $LiPF_6$-based electrolyte [43], [46]. b) Schematic open-circuit diagram of an aqueous electrolyte [46].

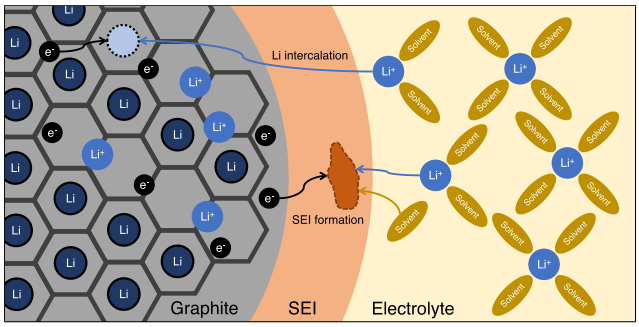

FIGURE 3. SEI Formation by interaction of Li^+ ions with electrolyte solvents and electrons during charging [61].

and the Lowest Unoccupied Molecular Orbital (LUMO). The electrolyte is reduced if the electrochemical potential of the anode (μ_A) is above the LUMO and, likewise, the electrolyte is oxidized if the electrochemical potential of the cathode (μ_C) is below the HOMO [63]. Because the electrochemical potential of graphite anodes falls outside the stability window of organic electrolytes, when the anode comes in contact with the electrolyte for the first time, the latter is reduced and decomposed onto the former, resulting in the SEI formation [64]. The SEI protects the negative electrode against solvent decomposition at a large negative voltage. A schematic of this behavior can be observed in Figure 2, where a) depicts the relationship between the potential and the specific capacity of various electrode materials and b) the schematic open-circuit diagram of an aqueous electrolyte. As it can be seen, the kinetic stability is reached by the SEI layer formation if $\mu_A > LUMO$ and/or $\mu_B > HOMO$.

Ideally, the SEI would be a layer that is both ion-conductive and electron-insulating, limiting additional electrolyte reduction at the anode while permitting reversible ion intercalation into it [40], [62], [63], [64]. The SEI is a multi-layered mosaic-like structure consisting of. firstly, an inorganic inner layer near the anode-SEI interface that allows Li^+ transport and, secondly, an organic heterogeneous outer layer at the SEI-electrolyte interface that is porous and permeable to both Li^+ and electrolyte solvent molecules [65]. Due to its porous nature, after the formation cycle, a small amount of electrolyte can still diffuse across the SEI layer and be reduced on the electrode surface, resulting in uninterrupted thickening of the SEI and continuous LLI [48]. This loss of active lithium causes the cell's capacity to drop irreversibly, while the thickening of the film layer causes an increase in IR [47], [61], [66]. Figure 3 depicts how the SEI is formed by the interaction of Li^+ ions with electrolyte solvents and electrons when they are transported through the electrolyte and intercalate into graphite during charging.

2) EFFECT OF TEMPERATURE & C-RATE

At high temperatures, firstly, the SEI shows increased degradation as it breaks down or dissolves, which may lead to subsequent restructuring of the damaged SEI or a re-precipitation of dissolved SEI products. Secondly, the SEI organic components shift towards more stable inorganic products, reducing the formation rate but also the ionic conductivity of the SEI [9]. Moreover, cycling at high C-rates causes increased ohmic heating, raising the temperature and leading the SEI to grow thicker on the negative electrode and its chemical composition to vary dramatically [67], [68]. The electrolyte may also evaporate as a result of ohmic heating, causing a buildup of pressure, which may result in cracks in the surface film. These fissures offer fresh locations for the lithiated carbon and electrolyte side reaction, further thickening the SEI layer [69].

3) EFFECT OF SoC

Furthermore, SoC also plays an important role in SEI growth. At increasing SoC, the potential imbalance at the anode/electrolyte interface favors the occurrence of electrolyte reduction reactions [12], promoting the formation of SEI [45]. However, in [70], it was found that the SEI growth rate does not increase steadily with SoC, but it

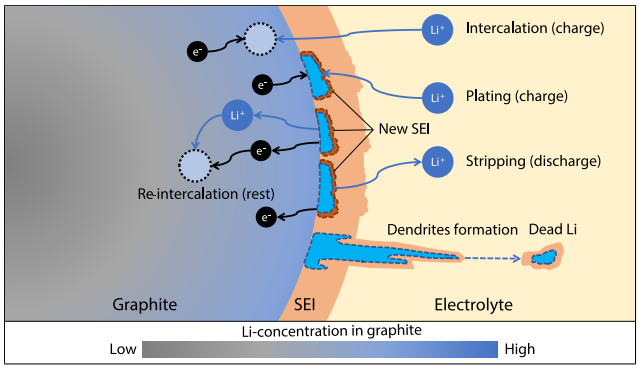

FIGURE 4. Li plating-stripping mechanism and its long-term consequences (dead Li and formation of dendrites). Based on a combination of [41], [71], [72].

is highly influenced by the graphite staging phenomena. Firstly, the electrode potential does not continuously vary with the SoC. Secondly, capacity fades due to electrolyte reduction, and SEI growth was found to be mostly constant in plateau regions covering SoC intervals between graphite stage transitions. When cells are cycled in SoC ranges containing graphite phase transitions, the anode surface suffers from dilation, causing the SEI to break and rebuild irreversibly [52].

4) EFFECT OF POTENTIAL & ANODE VOLUME CHANGES

Higher cut-off voltages also contribute to SEI formation and, hence, to greater battery aging. This is because higher and lower potentials are created in the positive and negative electrodes, respectively. Consequently, the electrolyte is oxidized more easily by the positive electrode's higher potential, and SEI is formed on the anode surface [73]. Finally, anode volume changes hasten the loss of lithium, further jeopardizing the SEI, especially during the first cycles, because significant structural disorder can modify the electrocatalytic properties and affect the SEi thickness and composition [74].

B. LITHIUM (LI) PLATING

1) DEFINITION & CAUSES

Lithium plating has been found to be a major source of LLI and LAM on the negative electrode [75]. It occurs under charging conditions at the surface of the negative electrode. The Li-graphite intercalation process is kinetically limited by two sources of overpotential:

- **Charge-transfer overpotential**: It appears at the negative electrode surface as soon as a current is applied. The charge-transfer process involves the ion de-solvation step before entering the SEI and the diffusion step through the SEI layer before receiving an electron at the electrode-SEI interface [76].
- **Solid diffusion overpotential**: The inserted lithium diffuses through the anode according to Fick's law, with the Li concentration in the solid phase determined based on the number of available sites. This mass transport is characterized by a solid diffusion coefficient following an Arrhenius-type temperature dependence [77].

Due to these overvoltage sources, if the current of Li^+ ions in the electrolyte exceeds the intercalation current or the transport rate inside graphite, the electrode potential drops below 0 V vs. Li^+/Li, leading to partial deposition of Li metal on the anode surface [78]. Under these conditions, the two reactions listed below coexist [77], [78]:

$$x\mathrm{Li}^+ + \mathrm{Li}_\delta\mathrm{C}_6 + x\mathrm{e}^- \longrightarrow \mathrm{Li}_{\delta+x}\mathrm{C}_6 \quad (1)$$

$$(1-x)\mathrm{Li}^+ + (1-x)\mathrm{e}^- \longrightarrow (1-x)\mathrm{Li}^\circ \quad (2)$$

where reaction (1) and reaction (2) are the insertion and deposition reactions, respectively, and $Li_\delta C_6$ denotes the lithiated graphite. Instead of intercalating into the anode crystal structure, Li ions are reduced to metallic Li, which deposits between the active material and the SEI, causing clogging of anode pores and potentially forming dendrites [42], [49]. As it can be observed in Figure 4, Li^+ ion concentration is larger towards the graphite surface since upon charging and discharging, they gradually intercalate from the core to the interface and deintercalate from the interface to the core, respectively. A secondary SEI layer is formed upon cycling around the plated Li.

Additionally, two further reactions may take place regardless of the external current:

$$\mathrm{R} + \mathrm{Li}^\circ \longrightarrow \mathrm{R\text{–}Li} \quad (3)$$

$$\varepsilon\mathrm{Li}^\circ + \mathrm{Li}_{\delta+x}\mathrm{C}_6 \longrightarrow \mathrm{Li}_{\delta+x+\varepsilon}\mathrm{C}_6 \quad (4)$$

Deposited metallic lithium may reduce the carbonate solvent electrolyte R to form additional SEI according to reaction (3), where Li° denotes the plated lithium [77]. The redundant SEI film formed, and the clogging of pores caused by deposited Li reduce the anode surface area, which in turn increases current densities at the remaining available pores, enhancing the likelihood of further lithium plating [43], [79]. However, a reversible portion of deposited Li may be recovered during electrode relaxation via re-intercalation into graphite [80], [81], following reaction (4). Stripping may also occur when part of the plated Li is re-oxidized and dissolved during discharge [78], [82]. Deposited metallic lithium may build up to develop dendrites, which are more prone to lose electrical contact with the anode and form floating fragments in the electrolyte (dead lithium) [83].

2) EFFECT OF TEMPERATURE

Temperature is one of the major factors influencing Li plating. At low temperatures, the diffusion of Li ions into graphite is hindered [82], and the activation energy required for charge transfer is higher [84], leading to slower kinetics and greater polarization in the anode. In particular, the charge transfer process is described by two subprocesses: firstly, (de)solvation of Li^+ at the electrolyte-SEI interface and, secondly, migration of Li^+ through the SEI [85]. Lithium plating at low temperatures can be determined by the sluggish charge transfer process or the limited Li solid diffusion [83].

Moreover, the reduced ionic conductivity of the electrolyte at low temperatures contributes to slower kinetics. Yet, it is not a limiting factor in that the diffusion of Li^+ is much faster in the electrolyte than in graphite [86].

3) EFFECT OF C-RATE & CUT-OFF VOLTAGE

High C-rates and cut-off voltages are also important causes of Li deposition. At high C-rates, the accumulation of Li ions at the anode/electrolyte interface caused by the slow solid diffusion of Li^+ in graphite leads to a high concentration gradient of Li ions, resulting in Li plating if the concentration becomes saturated [83]. Overcharging induces accumulation of Li ions at the anode-electrolyte interface when the amount of Li transferred from the positive to the negative electrode exceeds the amount of Li that can be accommodated in the anode, resulting in metallic Li deposition on its surface [87].

C. OTHER DEGRADATION MECHANISMS: MECHANICAL STRESS ON ELECTRODES

1) DEFINITION

During intercalation/deintercalation of Li ions into the cathode and anode, the electrode particles suffer from volume changes and mechanical stresses [52]. Especially in graphite anodes, the volume increase can be as high as 10%, and most of it occurs during the first 20% of Li insertion [2]. A schematic of this process is depicted in Figure 5, where the intercalation stages of Li into graphite and their relationship with the potential can be seen. Stage I represents the state without anode volume change where the graphite structure remains unharmed according to the Daumas-Herold model. Upon prolonged cycling (Stages II-IV), the anode suffers severe structural disordering, modifying its electrocatalytic properties and affecting the thickness and composition of the SEI. This is due to the exposed graphite edge sites' reaction with the electrolyte to (re)form SEI [74], resulting in LAM and LLI. After Transition III-IV, the potential rises exponentially. Additionally, a mechanical strain may result in electrode particle cracking and getting electrically separated from the bulk material, further contributing to LAM [57]. Graphite exfoliation, electrolyte reduction, and/or gas evolution inside graphite due to mechanical stress have also been reported to cause accelerated degradation of the anode as indirect consequences of these strains [9].

2) EFFECT OF SOC

The main factor affecting structural degradation in the anode is the SoC range, namely the maximum and minimum SoC reached by a cell during cycling. As observed in Figure 5, traversed voltage plateaus (or graphite phase transitions) have a notable impact on cyclic aging, and less mechanical stress is placed on cells that do not shift between them [28], [52], [74]. Yet, there is no clear consensus about which phase transitions are more detrimental. Transition I-II takes place at around 50% SoC and is the first cause of voltage deviation, while Transition III-IV is responsible for the biggest step in voltage with respect to Li occupation [89]. The cells cycled in [52] at SoC ranges slightly above stage II resulted in a higher LLI with respect to other phase transitions, and the authors attributed the results to the high dilation suffered by the graphite particle surface at the threshold between stages I and II. On the other hand, it was demonstrated in [74] that cycling at potentials involving low lithium concentrations in Li_xC_6 ($0 \leq x \leq 0.16$) is a major cause of anode structural damage while cycling at potentials corresponding to stages I and II ($x \geq 0.33$) reduces the impact of structural disordering. In a later study, the authors of [28] found that cells crossing the maximum transition between plateaus at 17% SoC presented fast degradation, while those cycled between 40% and 60% SoC showed the lowest degradation rate.

3) EFFECT OF C-RATE

High C-rates during charging or discharging do not seem to have an impact on the mechanical stress put on the negative electrode, and although higher peak stresses have been observed at high C-rates, the dependence appears to be relatively weak [90].

4) EFFECT OF BATTERY CHEMISTRY

Phase transitions also occur at the cathode during intercalation and deintercalation of Li ions, and the structural damage suffered by the cathode depends mainly on its chemistry [43]. LFP cathodes show a highly reversible transition between their $LiFePO_4$ and $FePO_4$ phases, and the degree of structural disorder reaches a maximum near the middle (mean SOC) of the charge/discharge cycle [19]. Yet, upon lithiation, its volume increase is not large compared to other chemistries, and hence, capacity fade caused by volume changes during cycling is slighter in this chemistry [22]. On the contrary, multiple phase transitions coexist in the NMC cathode voltage profile, which increases the difficulty of understanding the mechanisms involved in their structural degradation. The expansion and contraction of the NMC cathode structure can lead to primary and even secondary particle cracking upon cycling [53], [91]. Additionally, at high levels of delithiation, further structural disorders such as spinel structures due to non-ideal cation mixing may form [25], [26]. After extended charge/discharge cycles, ion-insulating cubic rocksalt phases may appear on the cathode surface [26], [27], in addition to the buildup of a complex surface film [27], [92], which can further increase capacity fade.

D. OTHER DEGRADATION MECHANISMS: TRANSITION METAL DISSOLUTION (TMD)

1) DEFINITION & EFFECT OF CHEMISTRY

A very significant challenge for transition metal-based cathodes is capacity and power fading, especially at high temperatures, which is directly related to the dissolution-migration-deposition (DMD) process of transition metal from the cathode materials [39]. LFP cathodes are commonly

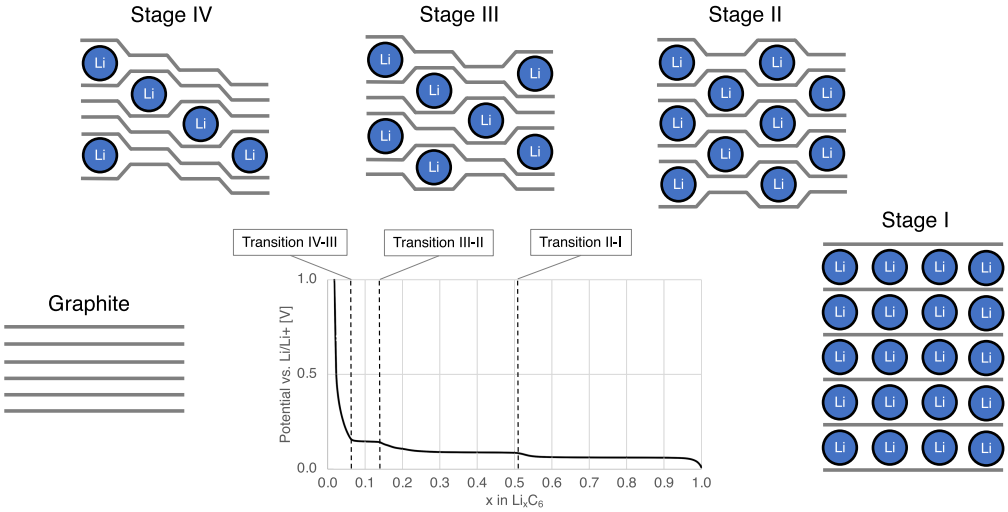

FIGURE 5. Daumas-Herold model of intercalation stages and transitions of Li into graphite. Based on a combination of [52], [74], [88].

doped with vanadium to improve electronic and ionic conductivity [93]. The bulk concentration of transition metals (Fe and V) declines in the cathode and increases in the anode as cells age, indicating the dissolution of these metals into the electrolyte and subsequent deposition onto the negative electrode surface, promoting the generation of surface layers and LAM [56]. Additionally, Fe and V serve as catalysts for SEI formation and growth reactions, consequently enhancing battery aging [20]. DMD of transition metals also takes place in NMC cathodes due to the presence of Mn because manganese ions are dissolved from the positive electrode onto the interface between the SEI and graphite. Consequently, the dissolved Mn ions create an oxygen-rich SEI layer comprising MN compounds, which negatively impacts battery capacity retention and coulombic efficiency and accelerates the formation of a less stable and greater SEI layer by impeding charge transfer [23], [54], [55].

2) EFFECT OF TEMPERATURE

Cathodic structural aging is also highly affected by temperature. Dissolution of Fe and subsequent formation of surface agglomerates at the cathode or deposition at the anode can be observed in LFP cells aged at high temperature, while low-temperature cycling can repress this mechanism [56]. At elevated temperatures, Mn dissolution in NMC cathodes is also higher [54].

3) EFFECT OF VOLTAGE

Extreme cut-off voltages also have an important impact on cathode structural degradation. Generally, the limiting factor is the oxidation potential of electrolyte solvents, which takes place at the high cathode (over)potentials [70], [94]. When the cathode material is completely delithiated, overcharging a LIB promotes heat generation and permanently damages the crystallographic structure of the cathode [95], potentially resulting in LLI and LAM. Under high cut-off voltage conditions, NMC cells studied in [26] showed surface structural degradation due to the formation of an ionically insulating layer on the cathode's surface, which tends to switch from a rhombohedral phase to a mixture of spinel and rock salt phases. Due to the rapid electrolyte decomposition that occurs at higher voltages, more acidic components are released, which can hasten the dissolution of NMC [96]. Very low cell voltages also contribute to degradation by promoting cathode particle cracking [97].

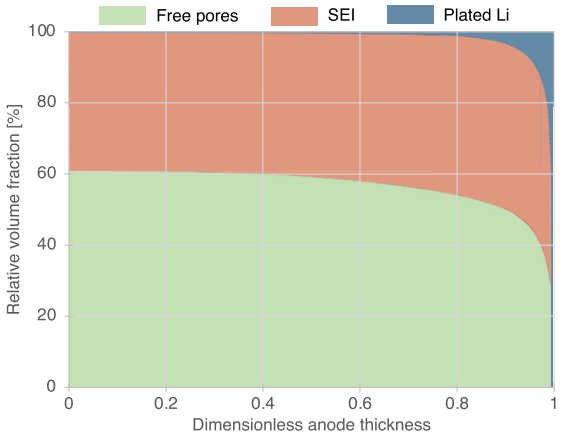

FIGURE 6. Relative volume fraction of free pores, SEI, and lithium metal across the anode after 3300 cycles [48].

E. INTERACTION OF DEGRADATION MECHANISMS CAUSING SATURATED AGING

As explained in Section I, among the various aging mechanisms studied in the literature, SEI formation and growth have traditionally been identified as the primary mechanism affecting the long-term degradation of LIBs [17], [47], [48]. In storage, a square-root dependency on time followed by

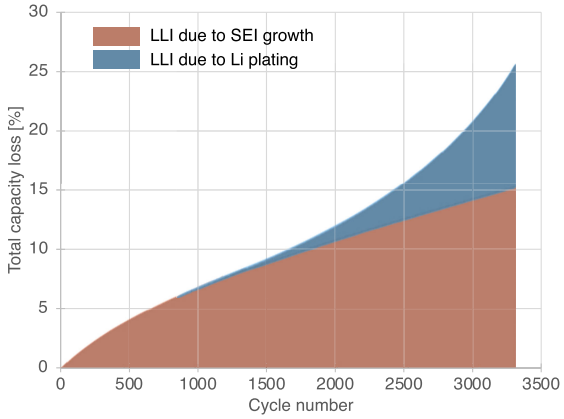

FIGURE 7. Variation of capacity loss in each cycle as a function of LLI due to SEI and Li plating over 3300 cycles [48].

capacity fade has been associated in several studies with SEI growth [29], [98], whereas, under cycling conditions, a linear component proportional to the charge throughput also arises [28], [48].

Nevertheless, a saturated degradation trend has been extensively reported after long-term cycling, resulting in sharp capacity decay and impedance rise once a certain number of cycles is reached [2], [17], [18]. Not only has saturated aging been reported in cells with different cathode chemistries, but large amounts of metallic Li were also detected at the anode surface in several aged cells [2], [99], leading some authors to attribute this abrupt saturated capacity fade behavior mainly to Li plating happening at the anode surface [48].

The dominant aging mechanism prior to the turning point (knee-point) is believed to be a thickening of the SEI catalyzed by oxidation products migrating to the anode. Afterward, due to decreased ionic kinetics and graphite active material degradation, lithium plating may occur even at low temperatures and charging rates [49]. The authors in [48] illustrated how the reduction of porosity is attributed to the growth of a surface film on the anode-separator interface, consisting of a combination of plated Li and SEI. Figure 6 shows how, near the separator of an aged cell, 40-50% of the initial pore volume is occupied by the SEI and a high amount of Li is plated at the very interface, resulting in a hindered ionic conduction and diffusion. Moreover, as it has been depicted in Figure 7, Li plating can be considered negligible in the early stages of cycling, and all the LLI is attributed to SEI growth. After a certain number of cycles, metallic Li begins to deposit on the anode surface, causing a drop in porosity, which in turn reinforces more Li plating. LLI by deposited Li increases exponentially with the cycle number at later stages, and the total aging rate increases when the LLI caused by plated Li exceeds the LLI caused by SEI formation (per-cycle) [48].

This interaction between deposited Li and the SEI is therefore responsible for the transition from stabilized to saturated behavior observed in the capacity fade curves of LIBs after prolonged cycling, ultimately rendering the battery early obsolete if the threshold between FL and SL is not carefully established. For this purpose, early identification of the knee-point is essential.

Overall, Figure 8 summarizes the degradation mechanisms that lead to LAM and LLI and their causes, based on the work in [10]. As depicted, most mechanisms lead to LAM, such as graphite exfoliation, transition metal dissolution, etc., while SEI formation and Li plating cause both LAM and LLI. Moreover, the high cell voltage and current (or C-rate) can be defined as the most hazardous causes, affecting most of the degradation mechanisms, e.g., SEI formation, electrolyte decomposition, graphite exfoliation, etc., followed by temperature and mechanical stress. Finally, the significance of the SEI formation and Li plating is also seen here since both are influenced by multiple factors simultaneously.

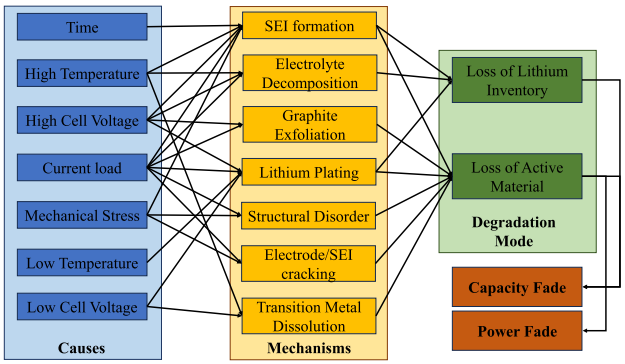

FIGURE 8. Summary of degradation modes, mechanisms, and causes that lead to capacity fade of LIBs [10].

III. KNEE-POINT IDENTIFICATION

Knee-points are defined by the IEEE standard as the point at which the capacity fade stops to decline stably (this occurs during most of the battery's life) and begins to decrease rapidly until the EoL [100]. This is the turning point depicted in Figure 1, which distinguishes the stabilization from the saturation stage (FL and SL, respectively). Both online and offline methods to identify the knee-point can be found in the literature: while online methods can identify the knee-point during operation based on data collected from previous cycles, offline identification of the knee-point requires the complete aging trajectory of the cell, making them less useful for models aiming at predicting the remaining life of LIBs still in use.

The authors in [101] described a methodology for offline detection of the knee-point by defining it as the cycle number of the intersection of two tangent lines on the capacity fade curve, obtained from the points with the minimum and maximum absolute slope-changing ratio of the capacity fade curve, following (5). Hence, the slow-changing ratio is defined as the difference in the curve slope at two consecutive

points divided by the slope at the initial point.

$$s(N) = \frac{l'(N+1) - l'(N)}{l'(N)} \tag{5}$$

where:
$s(N)$: curve on which the slope-changing ratio is assessed for each cycle N.
$l'(N)$: curve slope at the cycle interval [N-1, N].
$l'(N+1)$: curve slope at the adjacent cycle interval [N, N+1].

However, given the presence of derivatives of the fitted curve, the noise in the degradation curve caused by uncontrolled usage of the battery may have an impact on how well this gradient-based method performs.

Moreover, in [13], an offline detection methodology was used to identify the knee-point based on the Bacon-Watts model to estimate the transition between two intersecting straight lines, which does not rely on gradient methodologies and is claimed to be robust against noise. This model relates two straight lines to the left and right of an unknown transition point (the knee-point) as indicated in (6). In this work, the authors adjusted the model to identify two transitions instead of one in order to identify the knee onset.

$$Y = a_0 + a_1(x - x_1) + a_2(x - x_1)\tanh\left(\frac{x - x_1}{c}\right) + Z \tag{6}$$

where:
a_0: intercept of the leftmost segment.
a_1 and a_2: slopes of the intersecting lines.
c: abruptness of the transition.
x_1: knee-point.
Z: normally distributed and centered-in-zero random variable that represents the residuals.

In a more recent work [102], a knee-point detection approach was proposed to identify the knee-point both online and offline using raw capacity values without needing noise filtering. In order to achieve that, the authors defined a vector of straight lines Y_i superposed on the degradation curve, as dictated in (7), with their origin in the initial capacity and passing through the measured capacity in each cycle Q_i:

$$Y_i = \frac{(Q_i - Q_1)}{(i-1)}i + Q_1 \tag{7}$$

Y_i is subsequently subtracted from Q_i to generate the knee detection curve Kp_i. Finally, the knee detection curve is divided into two sections containing the same amount of points $Kp_{left,i}$ and $Kp_{right,i}$). The occurrence of the knee-point in the ith cycle is determined by (8):

$$i_{Kp} = i : (\overline{Kp_{left,i}} < \overline{Kp_{right,i}}) \tag{8}$$

When used offline, the average computational time required for detecting the knee-point with the technique proposed in [102] was reduced by 54.3% compared to [101] and by 91.2% compared to [13].

In [103], the normalized distance method was proposed to identify the knee-point as the most convex point in the shape of the aging curve. Additionally, it was concluded that the traditional state of health (SoH) of the battery (defined as the ratio of the current capacity divided by the nominal capacity of the LIB) is not sufficient to evaluate LIB aging in the linear zone. In order to account for the nonlinearities prevalent in LIB deterioration curves, they described the state of nonlinear aging (SoNA) as a more efficient health evaluation indicator that focuses on the full battery aging trajectory rather than a specific state point.

IV. NONLINEAR DEGRADATION MODELING

In recent years, several works have been published to predict LIBs' behavior in storage and under cycling conditions. Different approaches can be followed in order to achieve that, and different classifications can be found in the literature. Most review papers classify these models into a) empirical models, b) physics-based or electrochemical models, c) equivalent circuit models, and d) statistical or data-driven models [43], [104], [105]. Additional categorization can also be found in some publications, such as reduced-order models [106], [107], which could be understood as a subcategory of physics-based models.

When it comes to LIB degradation modeling, the aforementioned categories may be condensed into two major groups: physics-based models (PBM) and data-driven models (DDM). Equivalent circuit models can be considered PBM as they are a simplified yet less computationally expensive method to incorporate the underlying physics of a battery. Mathematical or empirical models, on the contrary, are DDM by definition, in that statistical methods such as linear regression or interpolation are used to predict future behavior without requiring in-depth knowledge of the underlying physics. In this work, an additional subcategorization is made between single-mechanism and multi-mechanism PBMs: whereas single-mechanism models focus solely on one of the degradation mechanisms discussed in Section II (therefore ignoring their interactions), multi-mechanism models incorporate two or more of those mechanisms, potentially improving model accuracy at the expense of increased complexity and computational cost.

A. SINGLE-MECHANISM PBMs

While a generally large series of assumptions are made when developing single-mechanism PBMs, they have been demonstrated to be a simple yet accurate tool to estimate the degradation of LIBs. Some authors have contributed models considering less prevalent aging mechanisms, such as the mechanical stress placed on negative electrodes during cycling [89], [108]. However, most of the literature in this field focuses on the two main aging mechanisms affecting LIBs, namely SEI formation and growth and Li plating.

1) SEI FORMATION AND GROWTH

As explained before, SEI formation protects the electrode from further reaction with the electrolyte. However, a small amount of electrolyte might still seep across this porous layer and be reduced at the anode surface, further thickening

the SEI [48] and enhancing battery aging. Consequently. the solvent diffusion rate slows as it thickens, reducing the SEI growth rate and fractional capacity loss [30]. In [29], the capacity fade was tracked as a function of storage temperature and time. By assuming that SEI growth is limited by electron migration across it, they developed an Arrhenius Law-based model, indicated in (9), which also accounted for the electronic conductivity and concluded that the cell capacity loss due to SEI growth has the following square root dependency with time:

$$t = e^{(A/T-B)}x^2 + e^{(C/T-D)}x \tag{9}$$

where:
t: time.
A, B, C and D: fitting factors obtained experimentally.
T: temperature.
x: LLI due to SEI formation.

Despite its simplicity and good accuracy, the main drawback of this model is that it only accounts for LLI by SEI growth as a cause of capacity loss.

The single SEI layer model developed in [30] also reflected a capacity fade with the square root of time. The authors assumed that at the anode-SEI interface, ethylene carbonate (EC) diffuses across the SEI and undergoes two-electron reduction, resulting in an insoluble product P, in turn increasing SEI thickness, which also grows proportional to the square root of time as indicated by (10).

$$x(t,T) = \frac{Z_P c_P A_a}{N_0} L(t) = \frac{Z_P c_P A_a}{N_0} 2\lambda \sqrt{D_{EC}(T)t} \tag{10}$$

where:
$x(t, T)$: fractional capacity loss.
Z_P: stoichiometric coefficient of Li in the insoluble product P.
c_P: molar density of the insoluble product P.
A_a: surface area of the anode.
N_0: initial capacity measured value.
$L(t)$: SEI thickness.
λ: factor dependant on the electrolyte composition and the molar volume of P.
D_{EC}: effective binary diffusivity of EC in P, dependent on the temperature T.
t: time.

The model accounted for continuously varying properties, including composition and porosity, providing a more sophisticated approach to SEI growth, yet again only accounting for LLI by SEI growth as a cause for capacity degradation.

The model developed in [31] also considered LLI due to solvent reduction reaction as the only cause for SEI growth and capacity fade. However, the authors accounted also for the contribution of the anode film resistance, enabling them to quantitatively study the effects of C-rate, DoD, and cut-off voltage. Based on the same premise, the work in [32] studied the influence of the SEI porosity on capacity fade with a new model that was able to simulate different aging profiles based on charge/discharge current rates and different storage open circuit voltage conditions (SOC).

In contrast, a two-layer SEI model was used in [109] to demonstrate that while transport of a charged species limits SEI growth, electronic leakage through the SEI is not the limiting mechanism. When formed at low potentials, the SEI passivates the anode more effectively, and for potentials greater than 0.3 V vs. Li/Li$^+$, growth of the SEI on glassy carbon is parabolic with time, consistent with capacity-fade measurements. They also found that the SEI densifies gradually and attributed transport and kinetics decrease to decreasing porosity rather than to increasing thickness.

The authors of [61] used a single-particle model to show that SEI formation is generally uniform on the anode surface, and heterogeneities can only be appreciated under very high C-rates. Again, an Arrhenius dependence was used to explain how temperature affects the diffusivity of the limiting reactive species through the SEI.

Moreover, a double-layer approach was used in [33] to explain the long-term SEI growth with finite porosity, concluding that its thickness and morphology can be predicted based on the structural properties. In the case that the formation of a dense SEI cannot be prevented, electron conduction is the rate-limiting mechanism in a situation in which electrons are conducted away from the electrode and solvent is diffused towards it, resulting in nearly constant porosity throughout the film and over time. Otherwise, solvent diffusion in the pores becomes the rate-limiting transport mechanism, and an inhomogeneous thickness distribution can be seen due to porosity fluctuations in the SEI. In a later paper [34], the diffusion of neutral lithium interstitials was identified as the limiting long-term growth mechanism [70].

In [111], the electrochemical kinetics of SEI growth were developed based on the assumption that the electronic conductivity of the initial SEI varies quadratically with the local lithium concentration, stimulating SEI growth during lithiation and suppressing it during delithiation. According to their findings, the SEI thickness is a complex function of transient variables such as cell potential, electron concentration, current direction and magnitude, and ion absorption energy. However, it was assumed that electron transport is the rate-limiting factor, which may only be valid for short periods of storage time, but no experimental data was provided to corroborate this assumption.

In the mixed model presented in [112], the authors predicted open circuit potential, SEI layer thickness, and capacity loss by accounting for solvent diffusion through the SEI and solvent reduction kinetics at the SEI/electrode interface, considering the effect of the initial SoC. Compared to previous work, they reported lower capacity loss and a thinner SEI due to its growth under open circuit conditions. They stated that the SEI growth depends on its own diffusion

TABLE 2. Comparison of Single-mechanism SEI growth models.

Model	Experimental fit	Stress factors	SEI model	Growth limiting factor
Brouselly et al. [29]	LCO/C and LMO/C	t, T	Single-layer model	Electronic conductivity in SEI
Ploehn et al. [30]	LCO/C and LMO/C [29]	t, T	Single-layer model	Solvent diffusion through SEI
Ning et al. [31]	LCO/MCMB	C-rate, DoD, cut-off V	Single-layer model	Solvent diffusion through SEI
Safari et al. [32]	LCO/C	C-rate, initial SoC	Single-layer model	Solvent diffusion through SEI Solvent reduction kinetics[1]
Tang et al. [109]	Glassy carbon anode	Potentiostatic	Two-layer model	Short time/higher potential: transport of a charged species Long time/lower potential: solvent reduction kinetics
Pinson et al. [61]	LFP/C (Liu et al. [110]	C-rate, T	Single-particle model	Solvent diffusion through SEI
Single et al. [33]	LCO/C and LMO/C [29]	t, T	Two-layer model	Low thickness: electronic conductivity in SEI High thickness: solvent diffusion through SEI
Single et al. [34]	NCA/C, NMC/C and LFP/C [70]	t, T, initial SoC	Two-layer model	Diffusion of Li intersticials
Das et al. [111]	Carbon black anode	C-rate, cut-off V	Single-layer model	Electron conductivity in SEI
Madi et al. [112]	Carbon anode [113]	t, initial SoC, solvent concentration	Single-layer model	Low thickness: solvent diffusion through SEI High thickness: solvent reduction kinetics

coefficient and thickness: the initial growth of the SEI layer is diffusion-limited, and after a certain thickness, the growth rate gradually slows down due to the rising resistance of the film, kinetically limiting the system.

A summary of the models compared in this subsection is included in Table 2.

2) LI PLATING

Li plating models are generally based on the kinetic limitations of the Li intercalation process into graphite, which in turn arise from the two sources of overpotential previously mentioned in subsection II-B, namely charge transfer and solid diffusion. The Butler-Volmer equation (11) (or variants like linearizations [114], [115]) has been widely used to model the charge transfer limitation effect on the Li deposition rate [15], [35], [37], [72], [77], [114], [115], [116], [117], [118], [119]:

$$j_{pl} = j_0 \left[\exp\left(\frac{\alpha_{a,k} F}{RT} \eta_{pl}\right) - \exp\left(\frac{\alpha_{c,k} F}{RT} \eta_{pl}\right) \right] \tag{11}$$

where:
j_{pl}: lithium plating local current density.
j_0: exchange current density.
$\alpha_{a,pl}$, $\alpha_{c,pl}$: anode and cathode transfer coefficients.
F: Faraday constant, equal to 96487 C·mol^{-1}.
R: universal gas constant, equal to 8.314 J·K^{-1}mol^{-1}.
T: temperature.
η_{pl}: local value of surface overpotential.

On the contrary, the diffusion of Li through a hypothetically spherical graphite particle is generally modeled according to Fick's second law in (12) [15], [77], [114], [115]:

$$\frac{\partial c_s}{\partial t} = \frac{D_s}{r^2} \frac{\partial}{\partial r} \left(r^2 \frac{\partial c_s}{\partial r} \right) \tag{12}$$

where:
c_s: solid phase concentration of Li in the particle.
D_s: solid phase diffusion coefficient.
R_s: particle radius.

One of the first Li plating models (based on a model previously developed in [120]) was used to study the effect of cell design parameters on Li deposition due to overcharging conditions and how it affects the resistance increase and capacity fade curves [35]. Their model allowed the authors to understand how plated lithium is spatially distributed across the negative electrode under different charging conditions, enabling them to establish operational and design limits that help avoid Li deposition. While the evolution of the SEI layer was not considered in the model, its resistance after the formation period was added as a constant value to the resistance of the film formed by metallic Li and Li_2CO_3 over time. They concluded that the risk of Li plating under overcharging conditions decreases in cells with an excess negative electrode compensating for the reduced specific capacity of the anode. In a later study [114], the overcharging conditions under which Li plating happens were investigated by means of a simplified two-dimensional model, concluding that the geometry of the anode with respect to the cathode plays an essential role in avoiding Li deposition. It was found that expanding it rather than increasing its thickness prevents Li deposition more effectively. However, in contrast with [35], the authors neglected the film resistances on electrodes in their model.

In [115], a control-oriented model suitable for BMS was developed based on a reduced-order approximation of the model in [35] capable of reducing the calculation time to 1/5000 compared to the physical-based model. In order to achieve this, the authors made a number of assumptions, such as constant local electrolyte and solid surface concentrations

[1] Kinetic-limited case failed to describe calendar aging.

TABLE 3. Comparison of Single-mechanism Li plating models.

Model	Experimental fit	Stress factors	Li plating model	Mechanisms considered
Arora et al. [35]	LMO/C	C-rate, cut-off V, electrode thickness	Macro-homogeneous model	Semi-reversible Li plating
Tang et al. [114]	LCO/C	C-rate, electrode geometry	Pseudo-2D model	Irreversible Li plating
Perkins et al. [115]	N/A	C-rate, initial SoC	Reduced order model	Irreversible Li plating
Legrand et al. [77]	LFP/C	C-rate, initial SoC	1D model (based on [121])	Irreversible Li plating
Tippmann et al. [15]	NMC/C	C-rate, T	Pseudo-2D ECT model	Irreversible Li plating
Ge et al. [116]	NMC/C	C-rate, T, SoC range	1D model	Irreversible Li plating
Carelli et al. [37]	LCO-NCA/C and NMC/C	C-rate, T, Li concentration	Pseudo-3D model	Reversible Li plating
Hein et al. [117]	Graphite anode	C-rate (current density)	3D model	Reversible plating
Hovestadt et al. [118]	NMC/C	C-rate	Pseudo-2D model	Reversible plating

(quasi-equilibrium state), uniform current density over the anode, and the same anodic and cathodic charge-transfer coefficients of the interalation kinetics. Furthermore, the work in [77] studied the risk of Li plating caused by charge transfer limitation as a function of the C-rate using a 1D electrochemical model previously developed in [121].

Additionally, the coupled electrochemical-thermal model developed in [15], parameterized for a wide range of temperature and SoC and validated against multiple discharge currents and driving profiles, showed a good correlation between experimental and semi-quantitative simulation results despite attributing all degradation to lithium plating. Their model enabled them to determine safe operational currents for each temperature and SoC. Moreover, the authors in [116] also determined safe operational limits for charging protocols by means of an electrochemical model, which allowed them to calculate lithium plating ratios (determined by the percentage of charge corresponding to Li plating and the total charge) for cells cycled at SoC ranges under 0 °C. According to their results, Li plating may also occur prior to the saturation of Li^+ ions concentration at the graphite surface. This is a consequence of the reduction of the surface potential due to the potential induced by the higher activation energy of Li^+ ion intercalation compared to that of Li plating. Such as in [35], they also accounted for the contribution of a constant SEI film resistance and a time-varying film resistance arising from the plating products (although only Li was considered).

In [37], an improved pseudo-3D model was used to simulate reversible Li plating based on the premise that the equilibrium potential of the plating reaction is not always equal to 0 V but varies as a function of local temperature, pressure, and concentration of Li^+ ions. Moreover, their model accounted not only for the intercalation and solid-state diffusion kinetics but also for the kinetics of the plating reaction itself, enabling them to generate operation maps over a wide range of C-rates and temperatures. An extensive experimental dataset was used for validation, showing good qualitative correlations; however, some quantitative differences were observed that might be related to the morphological characteristics of the deposited Li. A re-intercalation reaction was also included in their model as an alternative to the electrochemical oxidation of plated Li. In addition, a Li plating model was proposed in [117] that is independent of a transport model, allowing access to the spatial distribution of the lithium phase and permitting correlation of deposited Li to electrochemical features. Furthermore, plating onset could be recognized through a feature in the half-cell voltage during charge, which could serve as a characteristic indicator for battery diagnostics.

Finally, the model developed in [118] combined a pseudo-2D electrochemical model and a mechanical model to account for the pressure behavior of the cell during Li deposition while charging. This model was able to accurately reproduce experimental voltage and pressure data, predict Li plating onset based on measured pressure behavior, and optimize a fast charging protocol based on measured anode potential. A summary of the models reviewed in this subsection is available in Table 3.

3) KEY INSIGHTS

The key insights derived from the single-mechanism PB LIB degradation models can be summarized as follows:

a) Single-mechanism PBMs have been demonstrated to be a simple yet accurate tool to estimate the degradation of LIBs despite the large series of assumptions they often use.

b) It is commonly agreed that SEI growth modeling is reflected with a capacity fade with the square root of time.

c) While the transport of a charged species limits SEI growth, electronic leakage through the SEI is not the limiting mechanism.

d) SEI formation is mostly uniform on the anode surface, and the thickness and morphology of long-term SEI growth with finite porosity can be predicted based on the structural

properties. However, another study claims that SEI growth depends on its own diffusion coefficient and thickness.

e) Li plating models are generally based on the kinetic limitations of the Li intercalation process into graphite, and they are most often developed based on the Butler-Volmer equation.

f) The risk of Li plating under over-charging conditions decreases in cells with an excess negative electrode.

g) Li plating may also occur prior to the saturation of Li+ ions concentration at the graphite surface.

h) The half-cell charging voltage curve can recognize Li plating onset, which can serve as a characteristic indicator for battery diagnostics.

i) Most existing single-mechanism PB models consider either SEI formation/growth or Li plating. Time and temperature, followed by C-rate and initial SOC, are the main stress factors considered in the SEI formation models. On the contrary, C-rate is the respective main stress factor considered in the existing Li plating models, followed by temperature and initial SOC.

B. MULTI-MECHANISM PBMs

1) MODELS REVIEW

One of the first multidimensional models able to predict the spatial and temporal temperature distribution inside the cell by coupling the thermal and electrochemical behavior of the battery was developed in [122]. Despite the fact that the authors did not aim at predicting battery aging, their model would act as a benchmark for future physical-based modeling approaches. This model was later improved in [123] by incorporating features such as reversible, irreversible, and ohmic heating in matrix and solution phases, as well as the Arrhenius dependence of the various transport, kinetic, and mass-transfer parameters. This work also accounted for the entropic contribution of the manganese oxide spinel and carbon electrodes.

It was not until several years later that the first multi-mechanism aging models began to be developed. One of the earliest and most widely accepted ones was based on a linear combination of intact and cracked SEI layer [124]. The developed model used kinetics and transport control to describe the electrode kinetics, and despite showing a good correlation with the experimental results, its use was restricted to low C-rates (up to 1C) and a narrow temperature window (between 25 ^{o}C and 45 ^{o}C).

Moreover, in [125], the SEI growth and transition metal dissolution were combined as the dominating capacity fade mechanism for the anode and the cathode, respectively, the latter being assumed responsible for the saturated aging behavior. According to their model, the saturation in the capacity fade curve occurs when the LAM in the cathode is larger than the LLI caused by SEI growth. Additionally, the authors made a distinction between electronic and ionic conductivity within the SEI. Despite the accuracy of their model, they did not consider transition metal deposition on the anode and failed to implement Li plating as a second source of LLI, causing the slope after the knee-point to be underestimated by the model.

Furthermore, the electrochemical-thermal model previously developed in [122] was improved in [48] by accounting for both lithium plating and SEI growth and by incorporating the effect of anode porosity clogging too. Hence, the model was able to accurately characterize battery aging before and after the knee-point. It was confirmed that SEI is the dominant aging mechanism during the early stages of the battery. As the anode porosity reduces upon cycling, a larger gradient of electrolyte potential in the anode is formed and, consequently, a lower lithium deposition potential (LDP), leading to a saturated degradation stage dominated by irreversible Li plating. In their model, the authors used the following cathodic Tafel expression (13) to calculate the transfer current density of the lithium plating reaction:

$$j_{pl} = -a i_{0,pl} \exp -\frac{\alpha_{c,pl} F}{RT} \eta_{pl} \tag{13}$$

where:
a: specific surface area.
$i_{0,pl}$: exchange current density of lithium deposition, treated as a fitting parameter.
$\alpha_{C,pl}$: charge transfer coefficient.
F: Faraday constant, equal to 96487 C·mol^{-1}.
R: universal gas constant, equal to 8.314 J·K^{-1}mol^{-1}.
T: temperature.
η_{pl}: lithium deposition potential (LDP), defined in (14):

$$\eta_{pl} = \phi_s - \phi_e - \frac{j_{tot}}{a} R_{film} \tag{14}$$

where:
ϕ_s: solid phase potential (close to zero in the anode).
ϕ_e: electrolyte potential.
j_{tot}: total volumetric current density, defined as the sum of the current densities of the intercalation, SEI formation, and deposition reactions.
R_{film}: resistance of surface film (insignificant at room temperature).

Therefore, the LDP is highly dependent on the electrolyte potential at room temperature. In an aged cell's charging process, electrolyte potential is dramatically increased in the anode, especially in the region near the separator, consequently causing low LDP. Lithium plating occurs whenever the LDP goes below 0 V vs. Li/Li$^+$. Their model was even able to capture the voltage undershoot effect of a cell cycled at 3C after advanced aging, caused by a resistance increase due to local pore clogging near the anode/separator interface. Despite showing a very good correlation with experimental results, the model could still be more accurate if the effects of transition metal dissolution had also been included. Moreover, only irreversible lithium deposition was considered in their work. Therefore, the estimated fitting value of $I_{0,lpl}$ resulted in a lower than the actual exchange current density of Li metal stripping/plating. In a subsequent study [127], the same authors used their previous model to

TABLE 4. Comparison of multi-mechanism degradation models.

Model	Experimental fit	Stress factors	Model	Mechanisms considered
Ekström et al. [124]	LFP/C	C-rate, T	Single particle model	SEI growth SEI cracking
Kindermann et al. [125]	NMC/C	T, SoC	Pseudo-2D model	SEI growth Transition metal dissolution
Yang et al. [48]	NMC/C	C-rate	Pseudo-2D model (based on [122]	SEI growth Irreversible Li plating Anode porosity clogging
Ren et al. [72]	NMC/C	C-rate, T	Pseudo-2D model (based on [120])	SEI growth Reversible Li plating
Kupper et al. [126]	LFP/C	T, SoC range	Pseudo-3D model	SEI growth SEI cracking Electrode dry-out
Atalay et al. [36]	NMC/C [48]	C-rate	Pseudo-2D model	Heterogeneous dual-layer SEI growth Irreversible Li plating Anode porosity clogging Binary electrolyte (EC + DMC)
Carelli et al. [38]	LCO+NCA/C	C-rate, T	Pseudo-3D model	SEI growth (based on [126]) SEI cracking (based on [126]) Reversible Li plating (based on [37]) Irreversible Li plating
Sun et al. [119]	NMC/C	C-rate, T	3D model	SEI growth Reversible Li plating Irreversible Li plating

obtain an optimal temperature at which the battery should be operated in order to maximize the cycle life by minimizing both SEI formation and Li plating.

Additionally, an electrochemical model was developed in [72], which was capable of simulating the characteristic voltage plateau during relaxation after charging to investigate the reversibility of Li plating at low temperatures. The authors concluded that voltage plateaus observed in the anode potential profiles are induced by Li stripping and re-intercalation reactions and that local minima exhibited in the differential voltage curves are linearly related to the amount of reversible Li. Moreover, the electrochemical model developed in [126] combined different aging mechanisms, namely the formation and growth of the SEI, particle cracking in the anode, and percolation losses of the electrolyte due to electrode dry-out. Their model ascribed saturated degradation to the loss of contact between the active materials and the electrolyte as a consequence of the dry-out of electrodes due to gas formation, which was in quantitative agreement with experimental data.

Furthermore, the work [36] later proposed a more complete approach based on multi-layered heterogeneous SEI growth, irreversible lithium plating, and reduction of anode porosity. The authors considered a binary electrolyte filling the porous components of the electrodes, composed of ethylene carbonate (EC) and dimethyl carbonate (DMC), and coupled their diffusion coefficient and that of Li-ion as a function of local porosity. Despite ohmic heat generation being disregarded in this work, a higher performance than previous models ([48], [111], [124]) was claimed by the authors.

In [38], the 3D modeling framework for reversible Li plating developed in [37] was coupled with the SEI model in [126]. The resulting model was adjusted to account for the intricate interplays between SEI growth and Li deposition positive feedback, enabling it to describe cell degradation over a wide range of temperatures and C-rates and to identify critical operation conditions.

Finally, in a more recent study [119], a 3D electrochemical model was presented to investigate the occurrence of inhomogeneous Li plating in large-format LIBs under low-temperature charging conditions. The spatial distribution of metallic Li on the anode was found to be highly dependent on local current densities and overpotentials. While the main goal was to understand the behavior of the Li plating-stripping process at low temperatures, the model also accounted for irreversible Li plating and SEI formation, as well as the interaction of plated Li with the electrolyte to thicken the SEI film. Thus, it can be considered one of the most comprehensive multi-mechanism models in the literature due to all of the above. The models described in this subsection have been summarised in Table 4.

2) KEY INSIGHTS

The key insights derived from the multi-mechanism PB LIB degradation models can be summarized as follows:

a) It is generally agreed that SEI formation is the leading degradation mechanism during the stabilized degradation

stage, while Li plating is mostly responsible for the saturated degradation stage.

b) Hence, failing to include mechanisms such as Li plating or transition metal deposition or Li plating can be insignificant for the FL modeling of the LIB degradation; however, the SL can be highly underestimated, and the knee-point identification can be inaccurate.

c) C-rate is the main stress factor considered, followed by SOC and temperature, while SEI formation and growth is the mechanism always accounted for, followed by Li plating, in the multi-mechanism models.

d) Lithium deposition potential modeling is highly dependent on the consideration of the electrolyte potential at room temperature.

e) Voltage plateaus in the anode potential profiles are induced by Li stripping and re-intercalation reaction.

f) A main cause of saturated degradation (SL) is the loss of contact between the active materials and the electrolyte as a consequence of the dry-out of electrodes due to gas formation.

g) The spatial distribution of metallic Li on the anode is highly dependent on local current densities and overpotentials.

C. DATA-DRIVEN MODELS

Although PBMs aid in understanding how LIBs age from a physics perspective, they are not the sole approach to forecast long-term degradation. Data-driven approaches generally rely on large datasets of features typically based on measurable magnitudes such as current, voltage, or temperature, which, combined with statistical methods, enables estimation of the future physical behavior of the cell without explicitly making use of physics-based equations.

The advantages and disadvantages of PBM and data-driven approaches are already well-known in the literature. On the one hand, PBMs are capable of providing a better interpretation of the underlying physical laws and their relation with the results, while they also do not need historical data for their functionality. They can also provide generalized solutions, which are not highly case-specific. However, they are usually characterized by high complexity and computational time. Moreover, it is challenging to model the interdependencies between the various aging mechanisms, especially for LIB degradation. On the other hand, data-driven approaches are able to reduce computational time, provide accurate results regardless of the aging interdependencies, and inherently manage uncertainties. However, they need a large amount of historical data, and they are not easily applicable to different operating conditions and chemistries [129].

For online estimation of a battery's remaining useful life (RUL), two general DDM trends are currently followed in the literature [130]: the first one consists of using a previously developed lifetime model to estimate the RUL using historical battery usage data as input. On the contrary, the second approach relies on a prediction model fed with present battery characteristics data. In both cases, the design and appropriate training of these models is fundamental. Statistical models are generally simple to use and are characterized by high accuracy; however, they usually need comprehensive data (e.g. extensive battery behavior tests). On the contrary, machine learning (ML) models are more robust and more able to address the non-linearities of battery aging while maintaining high accuracy; however, they highly depend on the quantity and quality of the data, and they are usually characterized by a high computational time challenging their online implementation in real-world applications [131]. While most statistical and machine learning models currently focus on solely forecasting the RUL of the battery, few of them aim at predicting other parameters such as the knee-point or the elbow-point, and, to the best of our knowledge, none of them provide detailed insight about the behavior of the capacity fade/resistance increase curves during the saturated degradation stage. Under environmental and load conditions different from the training datasets, it is still challenging to reliably anticipate when a battery will reach the end of its useful life using state-of-health (SOH) predictions.

1) REGRESSION-BASED METHODS

Some works used regression-based approaches to estimate the RUL of LIBs. In [128], 124 lithium-iron-phosphate/graphite cells were tested under different conditions aiming at developing an elastic-net-based model able to accurately predict capacity degradation over time. The cells were cycled under various charge C-rates (1C to 8C), following 72 different one-step and two-step charging policies. Cell voltages, currents, and temperatures were measured during the test, and the authors found that the discharge capacity vs. voltage curves Q(V) and their derivatives (e.g. the difference of the discharge capacity curves vs voltage) are a rich data source effective in degradation diagnostics, as depicted in Figure 9. Indeed, by training the model with the variance of the change in discharge voltage curves between cycles 10 and 100 $\Delta Q_{10-100}(V)$, they were able to quantitatively predict the cycle life (Figure 9c) with an average percent error not higher than 15%. Moreover, by enhancing the features of the elastic-net model, they were able to reach average percent errors as low as 7.5%. Furthermore, they developed a classification model based on regularized logistic regression able to categorize cells into high- and low-lifetime with an accuracy of 95.1% using features from only the first 5 cycles.

Using the same dataset of [128] as input for their work, the authors in [132] developed a Gaussian Process Regression (GPR) model capable of estimating changes in the SoH of the battery by feeding it with features selected automatically and prioritized based on their impact in degradation. This enabled their model to accurately predict the entire capacity fade trajectory, knee-point, and EoL. Additionally, a migrated GPR was used in [133] to predict the two-stage aging trajectory of NMC LIBs. The model was fed offline with

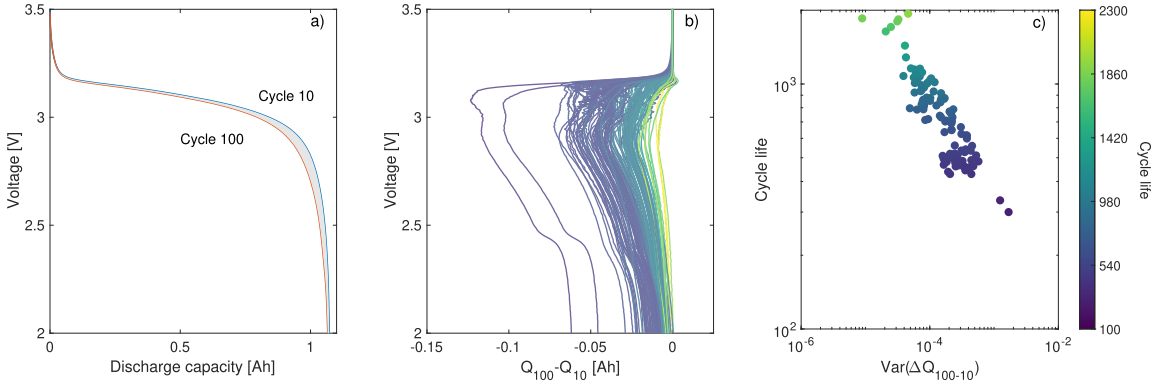

FIGURE 9. Features based on voltage curves from the first 100 cycles of the A123 dataset in [128]. (a) Discharge capacity curves for the 10th and 100th cycles for a representative cell. (b) Difference of the discharge capacity curves as a function of voltage between the 100th and 10th cycles, $\Delta Q_{100-10}(V)$. (c) Cycle life plotted as a function of the variance of $\Delta Q_{100-10}(V)$, with a correlation coefficient of −0.93.

accelerated-speed aging data of three batteries from different manufacturers, enabling them to achieve high-accuracy online aging predictions from the initial 30% data.

The use of regression-based methods (e.g. GPR) is increasing in LIB degradation prediction due to their non-parametric character and high flexibility in encompassing the non-linearities of the capacity fading while also being capable of directly quantifying the uncertainty levels in their prediction [131]. However, they are usually computationally expensive, and the proper selection of the appropriate Kernel function greatly affects the results. Hence, it is recommended that the model parameters and quantity and quality of the input data must be carefully considered for high prediction robustness [44].

2) NEURAL NETWORK-BASED METHODS

Neural networks (NNs) are often adopted to estimate the generally nonlinear degradation process of LIBs thanks to their superior ability to approximate nonlinearities, despite having a tendency to fall into local minima and frequently needing very large amounts of training data [134]. Two NN approaches are widely found in the literature for battery degradation purposes:

- Recurrent Neural Networks (RNNs) process sequences by iterating through the sequence elements and maintaining a state containing information relative to what it has seen so far [135].
- Convolutional Neural Networks (CNNs) work by learning a hierarchy of modular patterns and concepts to represent data [135].

Concerning RNNs, the study in [136], in order to account for the dynamic state behavior of LIBs, used an adaptive recurrent neural network (RNN) to predict their RUL, in which the network weights were adaptively optimized by means of the recursive Levenberg-Marquardt method. Furthermore, an RNN was used in [137] to monitor the SoH and predict the deterioration of high-power LIBs. In order to achieve that, the authors first developed an equivalent circuit model based on electrochemical impedance spectroscopy measurements to account for the dependence of internal resistance and open circuit voltage on the SoC. The work in [138] also developed a RUL prediction model based on Long Short-Term Memory RNN combined with Monte Carlo simulations. More recently, an LSTM sequence-to-sequence (S2S) RNN was used in [139] capable of detecting intrinsic variability caused by manufacturing differences to predict cell-specific EoL and knee-point from the first 100 cycles, and the model was validated with a dataset consisting of 48 NMC/C cells aged under the same conditions. The authors reported a notable increase in accuracy and computing speed compared to other state-of-the-art models.

On the contrary, CNNs have been increasingly used by several authors in recent years to predict the degradation trends of LIBs. In the work of [140], a CNN is proposed capable of predicting both the full capacity fade and internal resistance rise trajectory from only one cycle among the first 100 cycles of data. Their CNN employed convolutional feature extraction to eliminate the need for manual feature generation. In contrast, a classification model was proposed in [141] based on a CNN able to predict the knee-point online under a more realistic charge/discharge scenario. Their model was based on a two-stage approach: it first predicted whether or not a certain cell would reach the knee-point within the next 100 cycles with an accuracy of 91%, followed by an estimation of the remaining number of cycles before reaching the knee-point with a 14.6% mean absolute percent error (MAPE).

As explained, the main advantages of NNs are their high suitability for non-linear problems such as LIB aging and their high accuracy levels, while RNNs are also highly qualified for long-term forecasting (use of LSTM) [131]. However, their performance greatly depends on the training process and dataset, they are limited regarding uncertainty handling, while they can also cause overfitting issues. Therefore, the use of a high number of features is recommended for higher knowledge of the battery dynamics or the combination of several NNs for improved estimation results [44].

3) CLASSIFIERS

Support Vector Machines (SVMs) are a family of generalized linear classifiers that include a number of closely similar supervised learning techniques for classification and regression [142]. In [143], an SVM was used to estimate the RUL and SOH of LIBs and validate their model on driving profiles and temperatures not present during training. Moreover, an SVM-based model was developed in [144] to predict the SoH of LIBs at constant temperature and over an SoC range typical for EV operating conditions, solely based on current, voltage, and temperature training data. More recently, the authors in [13] employed an SVM for the early classification of cells by knee-point occurrence, enabling their model to categorize cells into "short," "medium," and "long-range," reaching an accuracy of 88% by using data from just the first 3 cycles.

SVMs do not require as much training data as NNs, and they are non-parametric and highly adaptable, making their solution global and unique within a short prediction time [131]. However, for RUL applications, SVMs have the disadvantage that they must select the proper kernel function, and only the point estimate value of the RUL is provided, whose uncertainty is difficult to determine [134]. Moreover, the utilized hyper-parameters need to be cross-validated, and the handling of the battery aging non-linearities is usually a challenge. Therefore, it is recommended that SVMs be used as a hybrid method component (e.g. SVMs and regression-based approaches) for performance improvement in applications as non-linear as the LIB degradation [44].

On the contrary, Relevance Vector Machines (RVMs), which have the same functional form as SVMs, are built using a Bayesian framework of extended linear models [142], resulting in probabilistic outputs capable of providing better generalization performance than SVMs. The study in [145] used an RVM to generate representative training vectors from capacity degradation data, which were later used to generate a capacity model able to calculate the failure threshold and estimate the RUL of a battery set. Their training dataset was, however, not very broad, consisting only of constant C-rate and constant temperature degradation curves, and their model was unable to dynamically update. To address these issues, the authors in [146] implemented an online training strategy in their RVM algorithm, achieving better prediction precision and improving the operating efficiency of RUL estimation. Also, in [13], an RVM was used for early quantitative prediction of knee-onset and knee-point using data from the first 50 cycles with a 12% and 9.4% error, respectively.

RVMs are characterized by a high degree of generalization and sparsity while they are also able to provide probability distribution functions (PDFs) as an output [131]. However, they need a very high amount of available data, and overfitting issues often occur. Therefore, it is recommended that the quality of the data is carefully considered and the data are pre-processed to avoid overfitting.

4) SEMI-SUPERVISED LEARNING

As already explained, data-driven approaches are often chosen over PB for LIB degradation due to the high modeling complexity of the various degradation mechanisms and their interactions. However, the previously described DD approaches, summarized also in Table 5, usually rely on a heavy amount of available labeled data collected, e.g., at room temperature, which is unsuitable for real-world dynamic conditions and challenges the data collection process. As a consequence, their accuracy and reliability are often hindered [147], [148]. On the contrary, semi-supervised DD approaches can function with the need for less data that are unlabeled and can be derived by different LIB systems extending their suitability for different applications [149].

For example, the authors in [147] extracted three features (namely current rate, pseudo-differential voltage, and temperature) from the battery discharging profiles using only an amount of up to 15% labeled data. The approach used was a semi-supervised method, which comprised a bidirectional gate recurrent unit (biGRU) and a structured kernel interpolation GPR finding an RMSE error below 1.91%. Moreover, a semi-supervised adversarial deep learning (SADL) method was utilized for capacity estimation in [148] to transform voltage and current data to capacity increment features, finding an RMSE error below 2% for various battery types. Additionally, the LIB RUL estimation work in [150] recommended an NN that included one encoder and three decoder heads for the feature extraction within 25 operation cycles and only 2% labeled data. Consequently, datasets from 34 different LIBs that comprised more than 19900 cycles under dynamic operation conditions were used for the validation of the approach. Furthermore, the semi-supervised partial Bayesian co-training (PBCT) method used in [151] led to up to 21.9% higher accuracy concerning LIB lifetime prediction than other supervised-learning approaches (e.g. elasticnet method) while simultaneously being able to follow other key influential factors of LIB degradation. Finally, with the use of semi-supervised learning, the authors in [152] managed to predict the capacity fade of a LIB cell at three difference temperatures with an RMSE of 0.24% using the cell labeled dataset from only one. However, it must be noted that the development of semi-supervised learning methods is generally characterized by higher complexity than that of supervised learning.

5) KEY INSIGHTS

The key insights derived from the data-driven LIB degradation models can be summarized as follows:

a) Regression-based models, NN-based models (RNNs & CNNs), and classifiers (SVMs & RVMs) have been used as data-driven approaches for LIB degradation prediction. While NN-based approaches have a higher capability of capturing the non-linearities of LIB degradation, they need a large amount of available data. On the contrary, classifiers while needing less amount of data, the appropriate Kernel

function for degradation prediction of each LIB chemistry can be challenging.

b) While higher precision can often be achieved with the PB models, data-driven approaches generally offer a good trade-off between model accuracy and response, reducing the high computational requirements and complexity. However, data-driven approaches are more efficient for total LIB aging prediction but less efficient in predicting the impact of every degradation mechanism.

c) The majority of data-driven models aim at forecasting the RUL of the battery, and only a few also attempt to predict other parameters, e.g. the knee-point or the elbow-point.

d) The existing data-driven approaches do not provide specific information regarding how the capacity fade/resistance rise curves behave throughout the saturated degradation stage.

e) The lack of available physical input complicates the forecast of the knee-point and EoL using SoH predictions under different environmental and load variables from the training datasets.

f) Semi-supervised learning approaches can overcome the data collection challenge of supervised approaches that need a large amount of labeled data which can be inaccurate under dynamic operation conditions and/or for other LIB battery models.

D. COMBINED PHYSICS-BASED & DATA-DRIVEN METHODS

1) REVIEWED STUDIES

The complexity and computational demands of the PB approaches and the lack of physical interpretation and generalization of the DD approaches have led to the investigation of combined approaches that can take advantage of the merits of both families, offering potential advancements in both short- and long-term predictions of LIB lifetime. In [154], the authors explored the ease of implementation, advantages, limitations, and viability of different combined PB and machine learning (ML)-based architectures for LIB lifetime prediction, for which a summary is provided in Figure 10. The sequential integration approaches (A1, A2, and A3) preserve ML and PB modeling as independent components, making them compatible with existing methodology. An alternate option for integration is the hybridization of ML and PB modeling approaches, in which the borders between each modeling paradigm become hazy, such as physics-constrained ML (B1) or machine learning-accelerated PB modeling (B2). Architecture B1 is typically accomplished through physics-based penalty terms, utilized to improve predictions and capture physical spatiotemporal relations, or through a physics-guided network architecture design to help learn low-dimensional, physical representations. For battery health forecasting, a generative ML model could be trained with conservation laws to constrain model evolution or PDE-constrained inverse problems could be solved for constitutive relations from datasets. On the other hand, architecture B2 relies on physics-informed ML, exemplified by physics-informed neural networks (PINNs), to solve underlying nonlinear PDEs for dynamic battery models, pioneered in [155].

PINNs are described as neural networks that are trained to solve supervised learning tasks while respecting any given law of physics described by general nonlinear partial differential equations. For example, aging-correlated parameters, derived by a generalizable PB model, were used to inform the DNN in [156], achieving an RMSE of 11.42 cycles utilizing only a single charging curve. Furthermore, physicochemical simulations with a pseudo-two-dimensional Newman model and laboratory or EV field data were used for data generation to inform the PINN developed in [157]. While the PINN achieved a LIB SOH estimation with an RMSE error below 2% with the use of laboratory data, differences in current profiles and signal acquisition proved to be the main limitations for the model generalization to the EV field data. On the contrary, an equivalent circuit model was used to produce the integral voltage error, which, together with the feature of dynamic operation conditions, was sent as input to a back propagation NN, achieving an RMSE error of 1% in [158]. Additionally, the PINN developed in [159] comprised two different NNs, one for feature-to-SOH mapping and one for dynamic degradation modeling, from which the latter does not depend on the battery operation profiles and can be used with transfer learning to the degradation modeling of other LIBs. Finally, a physics-informed autoencoder was developed in [160] to combine an electrochemical model with a Bayesian NN to increase early battery aging identification and uncertainty management.

Apart from the use of PINNs for LIB SOH or RUL estimation, there are a number of existing works in the literature that investigated how ML methods could be used with different means to assist the understanding of battery degradation mechanisms. For example, a CNN was used in [161] to overcome the challenge of time-consuming on-board open-circuit voltage (OCV) data acquisition for LIB aging prediction. With the use of the CVV, parameters such as electrode capacities and initial SOCs were estimated with very high accuracy compared to the offline OCV tests. The OCV curves could be reconstructed with a RMSE below $15mV$. Additionally, the hybrid approach followed in [162] achieved, besides aging prediction of lithium-sulfur batteries, untangling intractable degradation chemistry parameters such as the ratio of electrolyte amount to high-voltage-region capacity E/Q_{high} which was defined as an undiscovered indicator of capacity fading of this type of batteries. Moreover, the authors in [163], in continuation of their work in [155] where they introduced the fundamental frameworks for NNs being informed by PDEs (PINNs), used the developed PINNs to discover hidden physic laws in the given dataset. In addition, the ML approach ''transfer learning'' can be utilized to transfer available model knowledge in different frameworks needing only a small amount of known data. An example can be found in [164] where an established battery model is

TABLE 5. Data-driven approaches comparison.

Prediction	Author	Data	Model	Inputs	Features	Metrics
EoL	Severson et al. [128]	First 100 cycles (124 LFP/C cells)	Elastic net ("variance" model)	V, I	Manual selection	MAPE: 11.4%
			Elastic net ("full" model)	V, I, t_{ch}, T, SoH	Manual selection	MAPE: 9.1%
EoL	Strange et al. [140]	1 of the first 100 cycles (124 LFP/C cells)	CNN	V, I	Convolutional feature extraction	MAPE: 8.8%
EoL	Greenbank et al. [132]	Unclear number of input cycles (147 LFP/C cells)	GPR	V, I, T	Automated feature extraction (every 12 h of cycling)	Median PE: 1.3%
EoL	Li et al. [139]	First 100 cycles (48 NMC/C cells)*	RNN (LSTM, S2S model)	SoH	No feature selection required	MAPE: 5.4%
Knee-point	Zhang et al. [153]	Variable input (32 LCO/C cells)	Quantile regression + MC simulation	IC curve	Area: NE_I, NE_{II} Height: NE_{II}	No metrics provided
Knee-point	Fermin-Cueto et al. [13]	First 50 cycles (124 LFP/C cells)	RVM	V, I, Q(V), T(V)	Manual selection	MAPE: 9.4 %
Knee-point	Strange et al. [140]	1 of the first 100 cycles (124 LFP/C cells)	CNN	V, I	Convolutional feature extraction	MAPE: 9.7%
Knee-point	Li et al. [139]	First 100 cycles (48 NMC/C cells)*	RNN (LSTM, S2S model)	SoH	No feature selection required	MAPE: 5.7%
Knee-point	Greenbank et al. [132]	Unclear number of input cycles (147 LFP/C cells)	GPR	V, I, T	Automated feature extraction (every 12 h of cycling)	Median PE: 1.3%
Knee-point	Sohn et al. [141]	3 consecutive cycles (124 LFP/C cells)	CNN	V, I	Convolutional feature extraction	MAPE: 14.6%
Knee-point	Liu et al. [133]	First 30% of available data (3 NMC/C cells)	Migrated-GPR	SoH	No feature selection required	MAPE: 1.3%
Lifetime classification (Low/high lifetime)	Severson et al. [128]	First 5 cycles (124 LFP/C cells)	L1 regularized logistic regression ("variance" classifier)	V, I	Manual selection	Accuracy: 88.8%
			L1 regularized logistic regression ("full" classifier)	V, I, t_{ch}, T	Manual selection	Accuracy: 95.1%
Lifetime classification (Low/medium/high)	Fermin-Cueto et al. [13]	First 3 cycles (124 LFP/C cells)	SVM	V, I, T	Manual selection	Accuracy: 88%
Lifetime classification (Low/medium/high)	Strange et al. [140]	1 of the first 100 cycles (124 LFP/C cells)	CNN	V, I	Convolutional feature extraction	Accuracy: 88%

transferred to a different type of LIB for SOH estimation, overcoming the various heterogeneities in different LIB systems (rated capacities, electrode materials, etc).

Furthermore, as Figure 11 depicts, the authors in [153] found that the incremental capacity curve of negative electrodes reveals three distinct peaks, each corresponding to a different region under the curve. The area of the third region and the height of the second peak can be used to quantify LLI, whereas the area of the first and second regions can be used to characterize LAM. While these three regions could only be precisely identified under low C-rate conditions (0.05C), detection of the NE_{II} was also possible under normal charging conditions (1C). In their work, they used quantile regression and Monte Carlo simulations to identify the knee-point based on the evolution of the height of NE_{II}. The advantage of using combined methods is the capability of combining the low computational time of the data-driven approaches with the reproducibility and generalization that characterize the electrochemical models at the expense of the complexity of the model development.

Finally, a review of the different ways that data-driven approaches can assist PB methods for LIB lifetime forecast (''grey box modeling'') can be found in [165]. In this work, and in agreement with the summary of Figure 10, the first main category is the assistance in the estimation and optimization of PB parameters (data-driven assisted PB models), such as parameter identification, development of reduced-order PB models, and uncertainty qualification. The second category is the ''physics-guided data-driven approaches,'' which assist PB models in constructing datasets with physical meaning, tracking and accelerating the calculation of the PB capacity fading results, or calculating the error between a physical degradation model and the estimation.

2) KEY INSIGHTS

The key insights derived from the combined DD and PB LIB degradation models can be summarized as follows:

a) Data-driven and physics-based approaches can be combined with various integration means, which are mainly categorized into, firstly, sequential integration, such as residual learning, transfer learning, and parameter learning, and secondly, hybrid integration; physics-constrained ML or ML-accelerated PB models (PINNs).

b) PINNs can combine the advantages of the two families, providing high accuracy, physical laws interpretation, and less need for available data; however, these come at the expense of complexity, while the computational time depends on the architecture.

c) The use of ML approaches, such as PINNs, for untangling undiscovered degradation parameters and physical laws

Type	Architecture	Description	Limitations
A1. Sequential Integration: Residual or Delta Learning	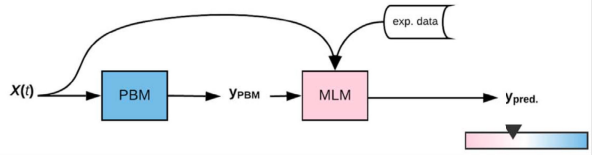	- MLM learns difference between PBM prediction and the measured y. - PBM is part of prediction pipeline.	- Limited to simpler PBM for online prediction. - Output partially constrained by known physics and applicability of PBM. - Prediction speed depends on PBM.
A2. Sequential Integration: Transfer Learning	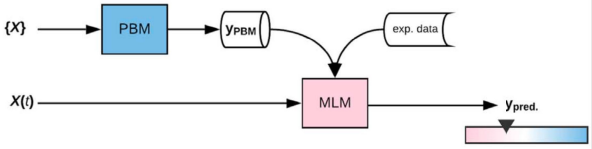	- MLM trains on exp. data augmented with PBM data. - PBM is not part of prediction pipeline. - Possible to use more complex PBM and MLM.	- Output partially constrained by known physics and applicability of PBM. - Generation of PBM data may have high computational cost.
A3. Sequential Integration: Parameter Learning	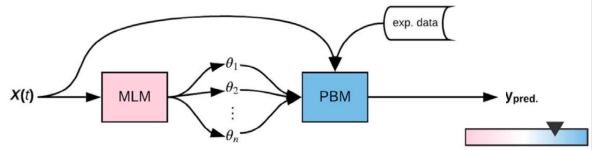	- MLM learns the parameters of a PBM that best explain the data. - Output strictly constrained by physics. - Features and results have interpretability.	- Complex to train. - Parameter identifiability can be important. - Prediction speed depends on PBM.
B1. Hybrid: Physics-constrained MLM	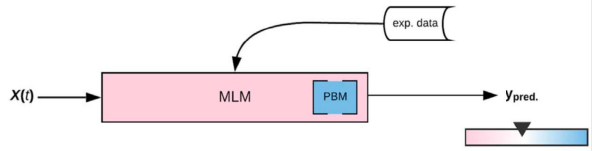	- MLM architecture contains physics-based elements by design (e.g. in loss function or NN architecture).	- Complex to design. - Can be data intensive (supplementable by Transfer Learning). - Output partially constrained by physics. - Prediction speed depends on PBM.
B2. Hybrid: ML-accelerated PBM	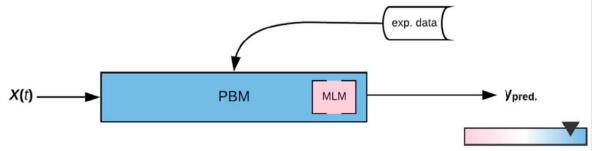	- ML-assisted solutions to PDEs in PBM. - ML guided data acquisition for PBM. - Can train complex model with small data. - Output strictly constrained by physics.	- Prediction speed depends on the architecture. - Extra steps may be needed to reproduce experimental data.

FIGURE 10. **Integration strategies for physics-based and machine learning models for forecasting battery health [154].**

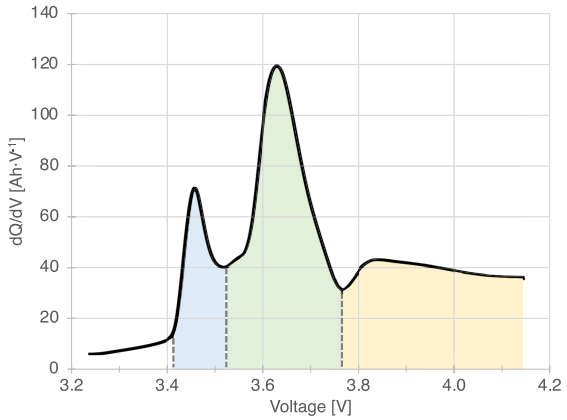

FIGURE 11. **Incremental capacity curve for an NMC battery charged at 0.05 C. The peak regions NE_I (blue), NE_{II} (green), and NE_{III} (yellow) are divided by the minima in the curve [153].**

in the input datasets is an emerging research direction that can provide valuable insights regarding the non-linearities and various interactive degradation mechanisms present in LIB degradation.

V. CONCLUSION AND FUTURE TRENDS

This work has, firstly, provided a detailed review of the main degradation mechanisms present in LIB aging, their causes and influencing factors. Secondly, the work focused on the summarization of the interrelations between the different aging mechanisms that cause the non-linear nature of the LIB capacity fading and the appearance of the so-called knee-point. Finally, the work contributed to the analysis and comparison of the existing single- and multi-mechanism physics-based and data-driven degradation model for LIB capacity fading and knee-point prediction. The LIB degradation understanding and the accurate knee-point identification are crucial for the safe LIB re-utilization in different applications (e.g. use of an EV LIB as stationary storage). While single-mechanism physics-based degradation modeling can be effective in FL prediction, the knee-point, and saturated aging can be significantly underestimated.

On the contrary, the modeling of the different mechanism interactions can be challenging in multi-mechanism models. Finally, data-driven models are proven to be effective for LIB aging prediction; however, the existing data-driven works are not focused on the identification of the knee-point of the degradation curve and they are not capable of distinguishing the various aging mechanisms.

In future research, the development of data-driven models with the aim of forecasting specific degradation parameters such as the knee-point is recommended. Moreover, it is proposed that further research of different combinations of physics-based and data-driven approaches is conducted for both enhanced LIB degradation prediction and discovery of unknown degradation parameters. Finally, online recalibration of data-driven approaches based on the behavior of the battery during operation (e.g. online knee-point recalculation in [102]) is also proposed for future research.

REFERENCES

[1] B. D. McCloskey, "Expanding the Ragone plot: Pushing the limits of energy storage," *J. Phys. Chem. Lett.*, vol. 6, no. 18, pp. 3592–3593, Sep. 2015, doi: 10.1021/acs.jpclett.5b01813.

[2] M. Broussely, P. Biensan, F. Bonhomme, P. Blanchard, S. Herreyre, K. Nechev, and R. J. Staniewicz, "Main aging mechanisms in Li ion batteries," *J. Power Sources*, vol. 146, nos. 1–2, pp. 90–96, Aug. 2005. [Online]. Available: https://www.sciencedirect.com/science/article/pii/S0378775305005082

[3] M. H. S. M. Haram, J. W. Lee, G. Ramasamy, E. E. Ngu, S. P. Thiagarajah, and Y. H. Lee, "Feasibility of utilising second life EV batteries: Applications, lifespan, economics, environmental impact, assessment, and challenges," *Alexandria Eng. J.*, vol. 60, no. 5, pp. 4517–4536, Oct. 2021. [Online]. Available: https://www.sciencedirect.com/science/article/pii/S1110016821001757

[4] E. Braco, I. San Martín, A. Berrueta, P. Sanchis, and A. Ursúa, "Experimental assessment of cycling ageing of lithium-ion second-life batteries from electric vehicles," *J. Energy Storage*, vol. 32, Dec. 2020, Art. no. 101695. [Online]. Available: https://www.sciencedirect.com/science/article/pii/S2352152X20315322

[5] S. Saxena, C. Le Floch, J. MacDonald, and S. Moura, "Quantifying EV battery end-of-life through analysis of travel needs with vehicle powertrain models," *J. Power Sources*, vol. 282, pp. 265–276, May 2015. [Online]. Available: https://www.sciencedirect.com/science/article/pii/S0378775315000841

[6] M. Philippot, D. Costa, M. S. Hosen, A. Senécat, E. Brouwers, E. Nanini-Maury, J. Van Mierlo, and M. Messagie, "Environmental impact of the second life of an automotive battery: Reuse and repurpose based on ageing tests," *J. Cleaner Prod.*, vol. 366, Sep. 2022, Art. no. 132872. [Online]. Available: https://www.sciencedirect.com/science/article/pii/S0959652622024659

[7] E. Martinez-Laserna, E. Sarasketa-Zabala, I. Villarreal Sarria, D.-I. Stroe, M. Swierczynski, A. Warnecke, J.-M. Timmermans, S. Goutam, N. Omar, and P. Rodriguez, "Technical viability of battery second life: A study from the ageing perspective," *IEEE Trans. Ind. Appl.*, vol. 54, no. 3, pp. 2703–2713, May 2018.

[8] C. R. Birkl, M. R. Roberts, E. McTurk, P. G. Bruce, and D. A. Howey, "Degradation diagnostics for lithium ion cells," *J. Power Sources*, vol. 341, pp. 373–386, Feb. 2017. [Online]. Available: https://www.sciencedirect.com/science/article/pii/S0378775316316998

[9] J. Vetter, P. Novák, M. R. Wagner, C. Veit, K. Möller, J. Besenhard, M. Winter, M. Wohlfahrt-Mehrens, C. Vogler, and A. Hammouche, "Ageing mechanisms in lithium-ion batteries," *J. Power Sources*, vol. 147, nos. 1–2, pp. 269–281, Mar. 2005. [Online]. Available: https://www.sciencedirect.com/science/article/pii/S0378775305000832

[10] X. Han, L. Lu, Y. Zheng, X. Feng, Z. Li, J. Li, and M. Ouyang, "A review on the key issues of the lithium ion battery degradation among the whole life cycle," *eTransportation*, vol. 1, Aug. 2019, Art. no. 100005. [Online]. Available: https://www.sciencedirect.com/science/article/pii/S2590116819300050

[11] C. Pastor-Fernández, T. F. Yu, W. D. Widanage, and J. Marco, "Critical review of non-invasive diagnosis techniques for quantification of degradation modes in lithium-ion batteries," *Renew. Sustain. Energy Rev.*, vol. 109, pp. 138–159, Jul. 2019. [Online]. Available: https://www.sciencedirect.com/science/article/pii/S136403211930200X

[12] A. Barré, B. Deguilhem, S. Grolleau, M. Gérard, F. Suard, and D. Riu, "A review on lithium-ion battery ageing mechanisms and estimations for automotive applications," *J. Power Sources*, vol. 241, pp. 680–689, Nov. 2013. [Online]. Available: https://www.sciencedirect.com/science/article/pii/S0378775313008185

[13] P. Fermín-Cueto, E. McTurk, M. Allerhand, E. Medina-Lopez, M. F. Anjos, J. Sylvester, and G. dos Reis, "Identification and machine learning prediction of knee-point and knee-onset in capacity degradation curves of lithium-ion cells," *Energy AI*, vol. 1, Aug. 2020, Art. no. 100006. [Online]. Available: https://www.sciencedirect.com/science/article/pii/S2666546820300069

[14] C. Strange, S. Li, R. Gilchrist, and G. dos Reis, "Elbows of internal resistance rise curves in Li-ion cells," *Energies*, vol. 14, no. 4, p. 1206, Feb. 2021. [Online]. Available: https://www.mdpi.com/1996-1073/14/4/1206

[15] S. Tippmann, D. Walper, L. Balboa, B. Spier, and W. G. Bessler, "Low-temperature charging of lithium-ion cells Part I: Electrochemical modeling and experimental investigation of degradation behavior," *J. Power Sources*, vol. 252, pp. 305–316, Apr. 2014. [Online]. Available: https://www.sciencedirect.com/science/article/pii/S0378775313019897

[16] J.-M. Tarascon and M. Armand, "Issues and challenges facing rechargeable lithium batteries," *Nature*, vol. 414, no. 6861, pp. 359–367, Nov. 2001, doi: 10.1038/35104644.

[17] M. Dubarry, C. Truchot, and B. Y. Liaw, "Cell degradation in commercial LiFePO4 cells with high-power and high-energy designs," *J. Power Sources*, vol. 258, pp. 408–419, Jul. 2014. [Online]. Available: https://www.sciencedirect.com/science/article/pii/S0378775314002365

[18] M. Lewerenz, J. Münnix, J. Schmalstieg, S. Käbitz, M. Knips, and D. U. Sauer, "Systematic aging of commercial $LiFePO_4$|graphite cylindrical cells including a theory explaining rise of capacity during aging," *J. Power Sources*, vol. 345, pp. 254–263, Mar. 2017. [Online]. Available: https://www.sciencedirect.com/science/article/pii/S037877531730143X

[19] C. T. Love, A. Korovina, C. J. Patridge, K. E. Swider-Lyons, M. E. Twigg, and D. E. Ramaker, "Review of $LiFePO_4$ phase transition mechanisms and new observations from X-ray absorption spectroscopy," *J. Electrochem. Soc.*, vol. 160, no. 5, pp. A3153–A3161, Apr. 2013, doi: 10.1149/2.023305jes.

[20] D. Li, D. L. Danilov, L. Gao, Y. Yang, and P. H. L. Notten, "Degradation mechanisms of the graphite electrode in C_6/$LiFePO_4$ batteries unraveled by a non-destructive approach," *J. Electrochem. Soc.*, vol. 163, no. 14, pp. A3016–A3021, Nov. 2016, doi: 10.1149/2.0821614jes.

[21] S. Sun, T. Guan, B. Shen, K. Leng, Y. Gao, X. Cheng, and G. Yin, "Changes of degradation mechanisms of $LiFePO_4$/graphite batteries cycled at different ambient temperatures," *Electrochimica Acta*, vol. 237, pp. 248–258, May 2017. [Online]. Available: https://www.sciencedirect.com/science/article/pii/S0013468617306540

[22] J. Hu, W. Huang, L. Yang, and F. Pan, "Structure and performance of the $LiFePO_4$ cathode material: From the bulk to the surface," *Nanoscale*, vol. 12, no. 28, pp. 15036–15044, 2020, doi: 10.1039/d0nr03776a.

[23] T. Li, X.-Z. Yuan, L. Zhang, D. Song, K. Shi, and C. Bock, "Degradation mechanisms and mitigation strategies of nickel-rich NMC-based lithium-ion batteries," *Electrochem. Energy Rev.*, vol. 3, no. 1, pp. 43–80, Mar. 2020, doi: 10.1007/s41918-019-00053-3.

[24] H. Kim, M. G. Kim, H. Y. Jeong, H. Nam, and J. Cho, "A new coating method for alleviating surface degradation of $LiNi_{0.6}Co_{0.2}Mn_{0.2}O_2$ cathode material: Nanoscale surface treatment of primary particles," *Nano Lett.*, vol. 15, no. 3, pp. 2111–2119, Mar. 2015, doi: 10.1021/acs.nanolett.5b00045.

[25] H. Gabrisch, T. Yi, and R. Yazami, "Transmission electron microscope studies of $LiNi_{1/3}Mn_{1/3}Co_{1/3}O_2$ before and after long-term aging at 70 °C," *Electrochem. Solid-State Lett.*, vol. 11, no. 7, p. A119, May 2008, doi: 10.1149/1.2919713.

[26] S.-K. Jung, H. Gwon, J. Hong, K.-Y. Park, D.-H. Seo, H. Kim, J. Hyun, W. Yang, and K. Kang, "Understanding the degradation mechanisms of $LiNi_{0.5}Co_{0.2}Mn_{0.3}O_2$ cathode material in lithium ion batteries," *Adv. Energy Mater.*, vol. 4, no. 1, 2014, Art. no. 1300787. [Online]. Available: https://onlinelibrary.wiley.com/doi/abs/10.1002/aenm.201300787

[27] Y. Ruan, X. Song, Y. Fu, C. Song, and V. Battaglia, "Structural evolution and capacity degradation mechanism of $LiNi_{0.6}Mn_{0.2}Co_{0.2}O_2$ cathode materials," *J. Power Sources*, vol. 400, pp. 539–548, Oct. 2018. [Online]. Available: https://www.sciencedirect.com/science/article/pii/S0378775318309157

[28] M. Ecker, N. Nieto, S. Käbitz, J. Schmalstieg, H. Blanke, A. Warnecke, and D. U. Sauer, "Calendar and cycle life study of $Li(NiMnCo)O_2$-based 18650 lithium-ion batteries," *J. Power Sources*, vol. 248, pp. 839–851, Feb. 2014. [Online]. Available: https://www.sciencedirect.com/science/article/pii/S0378775313016510

[29] M. Broussely, S. Herreyre, P. Biensan, P. Kasztejna, K. Nechev, and R. Staniewicz, "Aging mechanism in Li ion cells and calendar life predictions," *J. Power Sources*, vols. 97–98, pp. 13–21, Jan. 2001. [Online]. Available: https://www.sciencedirect.com/science/article/pii/S0378775301007224

[30] H. J. Ploehn, P. Ramadass, and R. E. White, "Solvent diffusion model for aging of lithium-ion battery cells," *J. Electrochem. Soc.*, vol. 151, no. 3, p. A456, Feb. 2004, doi: 10.1149/1.1644601.

[31] G. Ning and B. N. Popov, "Cycle life modeling of lithium-ion batteries," *J. Electrochem. Soc.*, vol. 151, no. 10, p. A1584, Sep. 2004, doi: 10.1149/1.1787631.

[32] M. Safari, M. Morcrette, A. Teyssot, and C. Delacourt, "Multimodal physics-based aging model for life prediction of Li-ion batteries," *J. Electrochem. Soc.*, vol. 156, no. 3, p. A145, Dec. 2009, doi: 10.1149/1.3043429.

[33] F. Single, B. Horstmann, and A. Latz, "Revealing SEI morphology: In-depth analysis of a modeling approach," *J. Electrochem. Soc.*, vol. 164, no. 11, pp. E3132–E3145, May 2017, doi: 10.1149/2.0121711jes.

[34] F. Single, A. Latz, and B. Horstmann, "Identifying the mechanism of continued growth of the solid–electrolyte interphase," *ChemSusChem*, vol. 11, no. 12, pp. 1950–1955, Jun. 2018. [Online]. Available: https://chemistry-europe.onlinelibrary.wiley.com/doi/abs/10.1002/cssc.201800077

[35] P. Arora, M. Doyle, and R. E. White, "Mathematical modeling of the lithium deposition overcharge reaction in lithium-ion batteries using carbon-based negative electrodes," *J. Electrochem. Soc.*, vol. 146, no. 10, pp. 3543–3553, Oct. 1999, doi: 10.1149/1.1392512.

[36] S. Atalay, M. Sheikh, A. Mariani, Y. Merla, E. Bower, and W. D. Widanage, "Theory of battery ageing in a lithium-ion battery: Capacity fade, nonlinear ageing and lifetime prediction," *J. Power Sources*, vol. 478, Dec. 2020, Art. no. 229026. [Online]. Available: https://www.sciencedirect.com/science/article/pii/S0378775320313239

[37] S. Carelli and W. G. Bessler, "Prediction of reversible lithium plating with a pseudo-3D lithium-ion battery model," *J. Electrochem. Soc.*, vol. 167, no. 10, Jun. 2020, Art. no. 100515, doi: 10.1149/1945-7111/ab95c8.

[38] S. Carelli and W. G. Bessler, "Coupling lithium plating with SEI formation in a pseudo-3D model: A comprehensive approach to describe aging in lithium-ion cells," *J. Electrochem. Soc.*, vol. 169, no. 5, May 2022, Art. no. 050539, doi: 10.1149/1945-7111/ac716a.

[39] C. Zhan, T. Wu, J. Lu, and K. Amine, "Dissolution, migration, and deposition of transition metal ions in Li-ion batteries exemplified by mn-based cathodes—A critical review," *Energy Environ. Sci.*, vol. 11, no. 2, pp. 243–257, 2018, doi: 10.1039/c7ee03122j.

[40] E. Peled and S. Menkin, "Review—SEI: Past, present and future," *J. Electrochem. Soc.*, vol. 164, no. 7, pp. A1703–A1719, Jun. 2017, doi: 10.1149/2.1441707jes.

[41] Y. Tian, C. Lin, H. Li, J. Du, and R. Xiong, "Detecting undesired lithium plating on anodes for lithium-ion batteries – a review on the in-situ methods," *Appl. Energy*, vol. 300, Oct. 2021, Art. no. 117386. [Online]. Available: https://www.sciencedirect.com/science/article/pii/S0306261921007893

[42] U. Janakiraman, T. R. Garrick, and M. E. Fortier, "Review—Lithium plating detection methods in Li-ion batteries," *J. Electrochem. Soc.*, vol. 167, no. 16, Dec. 2020, Art. no. 160552, doi: 10.1149/1945-7111/abd3b8.

[43] W. Vermeer, G. R. Chandra Mouli, and P. Bauer, "A comprehensive review on the characteristics and modeling of lithium-ion battery aging," *IEEE Trans. Transport. Electrific.*, vol. 8, no. 2, pp. 2205–2232, Jun. 2022.

[44] M. Elmahallawy, T. Elfouly, A. Alouani, and A. M. Massoud, "A comprehensive review of lithium-ion batteries modeling, and state of health and remaining useful lifetime prediction," *IEEE Access*, vol. 10, pp. 119040–119070, 2022.

[45] K. Liu, T. R. Ashwin, X. Hu, M. Lucu, and W. D. Widanage, "An evaluation study of different modelling techniques for calendar ageing prediction of lithium-ion batteries," *Renew. Sustain. Energy Rev.*, vol. 131, Oct. 2020, Art. no. 110017.[Online]. Available: https://www.sciencedirect.com/science/article/pii/S1364032120303087

[46] J. B. Goodenough and Y. Kim, "Challenges for rechargeable Li batteries," *Chem. Mater.*, vol. 22, no. 3, pp. 587–603, Feb. 2010, doi: 10.1021/cm901452z.

[47] J. Wang, J. Purewal, P. Liu, J. Hicks-Garner, S. Soukazian, E. Sherman, A. Sorenson, L. Vu, H. Tataria, and M. W. Verbrugge, "Degradation of lithium ion batteries employing graphite negatives and nickel–cobalt–manganese oxide + spinel manganese oxide positives: Part 1, aging mechanisms and life estimation," *J. Power Sources*, vol. 269, pp. 937–948, Dec. 2014. [Online]. Available: https://www.sciencedirect.com/science/article/pii/S037877531401074X

[48] X.-G. Yang, Y. Leng, G. Zhang, S. Ge, and C.-Y. Wang, "Modeling of lithium plating induced aging of lithium-ion batteries: Transition from linear to nonlinear aging," *J. Power Sources*, vol. 360, pp. 28–40, Aug. 2017. [Online]. Available: https://www.sciencedirect.com/science/article/pii/S0378775317307619

[49] S. F. Schuster, T. Bach, E. Fleder, J. Müller, M. Brand, G. Sextl, and A. Jossen, "Nonlinear aging characteristics of lithium-ion cells under different operational conditions," *J. Energy Storage*, vol. 1, pp. 44–53, Jun. 2015. [Online]. Available: https://www.sciencedirect.com/science/article/pii/S2352152X15000092

[50] J. Zhang, B. Lu, Y. Song, and X. Ji, "Diffusion induced stress in layered Li-ion battery electrode plates," *J. Power Sources*, vol. 209, pp. 220–227, Jul. 2012. [Online]. Available: https://www.sciencedirect.com/science/article/pii/S0378775312005265

[51] X.-G. Yang, C. Bauer, and C.-Y. Wang, "Sinusoidal current and stress evolutions in lithium-ion batteries," *J. Power Sources*, vol. 327, pp. 414–422, Sep. 2016. [Online]. Available: https://www.sciencedirect.com/science/article/pii/S0378775316309454

[52] S. Gantenbein, M. Schönleber, M. Weiss, and E. Ivers-Tiffée, "Capacity fade in lithium-ion batteries and cyclic aging over various state-of-charge ranges," *Sustainability*, vol. 11, no. 23, p. 6697, Nov. 2019. [Online]. Available: https://www.mdpi.com/2071-1050/11/23/6697

[53] H.-H. Ryu, K.-J. Park, C. S. Yoon, and Y.-K. Sun, "Capacity fading of Ni-rich $Li[Ni_xCo_yMn_{1-x-y}]O_2$ ($0.6 \leq X \leq 0.95$) cathodes for high-energy-density lithium-ion batteries: Bulk or surface degradation?" *Chem. Mater.*, vol. 30, no. 3, pp. 1155–1163, Feb. 2018, doi: 10.1021/acs.chemmater.7b05269.

[54] X. Xiao, Z. Liu, L. Baggetto, G. M. Veith, K. L. More, and R. R. Unocic, "Unraveling manganese dissolution/deposition mechanisms on the negative electrode in lithium ion batteries," *Phys. Chem. Chem. Phys.*, vol. 16, no. 22, p. 10398, 2014, doi: 10.1039/c4cp00833b.

[55] T. Joshi, K. Eom, G. Yushin, and T. F. Fuller, "Effects of dissolved transition metals on the electrochemical performance and SEI growth in lithium-ion batteries," *J. Electrochem. Soc.*, vol. 161, no. 12, pp. A1915–A1921, Sep. 2014, doi: 10.1149/2.0861412jes.

[56] M. Simolka, J.-F. Heger, H. Kaess, I. Biswas, and K. A. Friedrich, "Influence of cycling profile, depth of discharge and temperature on commercial LFP/C cell ageing: Post-mortem material analysis of structure, morphology and chemical composition," *J. Appl. Electrochem.*, vol. 50, no. 11, pp. 1101–1117, Nov. 2020, doi: 10.1007/s10800-020-01465-6.

[57] C. Zhan, J. Lu, A. Jeremy Kropf, T. Wu, A. N. Jansen, Y.-K. Sun, X. Qiu, and K. Amine, "Mn(II) deposition on anodes and its effects on capacity fade in spinel lithium manganate–carbon systems," *Nature Commun.*, vol. 4, no. 1, p. 2437, Sep. 2013, doi: 10.1038/ncomms3437.

[58] J. Lu, C. Zhan, T. Wu, J. Wen, Y. Lei, A. J. Kropf, H. Wu, D. J. Miller, J. W. Elam, Y.-K. Sun, X. Qiu, and K. Amine, "Effectively suppressing dissolution of manganese from spinel lithium manganate via a nanoscale surface-doping approach," *Nature Commun.*, vol. 5, no. 1, p. 5693, Dec. 2014, doi: 10.1038/ncomms6693.

[59] K. Edström, T. Gustafsson, and J. O. Thomas, "The cathode–electrolyte interface in the Li-ion battery," *Electrochimica Acta*, vol. 50, nos. 2–3, pp. 397–403, Aug. 2004. [Online]. Available: https://www.sciencedirect.com/science/article/pii/S0013468604006486

[60] M. Herstedt, M. Stjerndahl, A. Nytén, T. Gustafsson, H. Rensmo, H. Siegbahn, N. Ravet, M. Armand, J. O. Thomas, and K. Edström, "Surface chemistry of carbon-treated $LiFePO_4$ particles for Li-ion battery cathodes studied by PES," *Electrochem. Solid-State Lett.*, vol. 6, no. 9, p. A202, Jul. 2003, doi: 10.1149/1.1594413.

[61] M. B. Pinson and M. Z. Bazant, "Theory of SEI formation in rechargeable batteries: Capacity fade, accelerated aging and lifetime prediction," *J. Electrochem. Soc.*, vol. 160, no. 2, pp. A243–A250, Dec. 2012, doi: 10.1149/2.044302jes.

[62] K. Xu, "Nonaqueous liquid electrolytes for lithium-based rechargeable batteries," *Chem. Rev.*, vol. 104, no. 10, pp. 4303–4418, Oct. 2004, doi: 10.1021/cr030203g.

[63] S. J. An, J. Li, C. Daniel, D. Mohanty, S. Nagpure, and D. L. Wood, "The state of understanding of the lithium-ion-battery graphite solid electrolyte interphase (SEI) and its relationship to formation cycling," *Carbon*, vol. 105, pp. 52–76, Aug. 2016. [Online]. Available: https://www.sciencedirect.com/science/article/pii/S0008622316302676

[64] N. Takenaka, A. Bouibes, Y. Yamada, M. Nagaoka, and A. Yamada, "Frontiers in theoretical analysis of solid electrolyte interphase formation mechanism," *Adv. Mater.*, vol. 33, no. 37, Sep. 2021, Art. no. 2100574. [Online]. Available: https://onlinelibrary.wiley.com/doi/abs/10.1002/adma.202100574

[65] A. Wang, S. Kadam, H. Li, S. Shi, and Y. Qi, "Review on modeling of the anode solid electrolyte interphase (SEI) for lithium-ion batteries," *NPJ Comput. Mater.*, vol. 4, no. 1, Mar. 2018, Art. no. 15, doi: 10.1038/s41524-018-0064-0.

[66] J. de Hoog, J.-M. Timmermans, D. Ioan-Stroe, M. Swierczynski, J. Jaguemont, S. Goutam, N. Omar, J. Van Mierlo, and P. Van Den Bossche, "Combined cycling and calendar capacity fade modeling of a Nickel-Manganese-Cobalt oxide cell with real-life profile validation," *Appl. Energy*, vol. 200, pp. 47–61, Aug. 2017. [Online]. Available: https://www.sciencedirect.com/science/article/pii/S0306261917305251

[67] L. Somerville, J. Bareño, S. Trask, P. Jennings, A. McGordon, C. Lyness, and I. Bloom, "The effect of charging rate on the graphite electrode of commercial lithium-ion cells: A post-mortem study," *J. Power Sources*, vol. 335, pp. 189–196, Dec. 2016. [Online]. Available: https://www.sciencedirect.com/science/article/pii/S0378775316313842

[68] Y. Gao, J. Jiang, C. Zhang, W. Zhang, Z. Ma, and Y. Jiang, "Lithium-ion battery aging mechanisms and life model under different charging stresses," *J. Power Sources*, vol. 356, pp. 103–114, Jul. 2017. [Online]. Available: https://www.sciencedirect.com/science/article/pii/S0378775317305876

[69] G. Ning, B. Haran, and B. N. Popov, "Capacity fade study of lithium-ion batteries cycled at high discharge rates," *J. Power Sources*, vol. 117, nos. 1–2, pp. 160–169, May 2003. [Online]. Available: https://www.sciencedirect.com/science/article/pii/S0378775303000296

[70] P. Keil, S. F. Schuster, J. Wilhelm, J. Travi, A. Hauser, R. C. Karl, and A. Jossen, "Calendar aging of lithium-ion batteries," *J. Electrochem. Soc.*, vol. 163, no. 9, pp. A1872–A1880, Jul. 2016, doi: 10.1149/2.0411609jes.

[71] G. Zhang, X. Wei, G. Han, H. Dai, J. Zhu, X. Wang, X. Tang, and J. Ye, "Lithium plating on the anode for lithium-ion batteries during long-term low temperature cycling," *J. Power Sources*, vol. 484, Feb. 2021, Art. no. 229312. [Online]. Available: https://www.sciencedirect.com/science/article/pii/S0378775320316001

[72] D. Ren, K. Smith, D. Guo, X. Han, X. Feng, L. Lu, M. Ouyang, and J. Li, "Investigation of lithium plating-stripping process in Li-ion batteries at low temperature using an electrochemical model," *J. Electrochem. Soc.*, vol. 165, no. 10, pp. A2167–A2178, Jul. 2018, doi: 10.1149/2.0661810jes.

[73] L. Su, J. Zhang, C. Wang, Y. Zhang, Z. Li, Y. Song, T. Jin, and Z. Ma, "Identifying main factors of capacity fading in lithium ion cells using orthogonal design of experiments," *Appl. Energy*, vol. 163, pp. 201–210, Feb. 2016. [Online]. Available: https://www.sciencedirect.com/science/article/pii/S0306261915014555

[74] V. A. Sethuraman, L. J. Hardwick, V. Srinivasan, and R. Kostecki, "Surface structural disordering in graphite upon lithium intercalation/deintercalation," *J. Power Sources*, vol. 195, no. 11, pp. 3655–3660, Jun. 2010. [Online]. Available: https://www.sciencedirect.com/science/article/pii/S0378775309022964

[75] U. R. Koleti, A. Rajan, C. Tan, S. Moharana, T. Q. Dinh, and J. Marco, "A study on the influence of lithium plating on battery degradation," *Energies*, vol. 13, no. 13, p. 3458, Jul. 2020. [Online]. Available: https://www.mdpi.com/1996-1073/13/13/3458

[76] T. R. Jow, S. A. Delp, J. L. Allen, J.-P. Jones, and M. C. Smart, "Factors limiting Li+Charge transfer kinetics in Li-ion batteries," *J. Electrochem. Soc.*, vol. 165, no. 2, pp. A361–A367, Jan. 2018, doi: 10.1149/2.1221802jes.

[77] N. Legrand, B. Knosp, P. Desprez, F. Lapicque, and S. Raël, "Physical characterization of the charging process of a Li-ion battery and prediction of Li plating by electrochemical modelling," *J. Power Sources*, vol. 245, pp. 208–216, Jan. 2014. [Online]. Available: https://www.sciencedirect.com/science/article/pii/S0378775313011373

[78] C. Uhlmann, J. Illig, M. Ender, R. Schuster, and E. Ivers-Tiffée, "In situ detection of lithium metal plating on graphite in experimental cells," *J. Power Sources*, vol. 279, pp. 428–438, Jan. 2015. [Online]. Available: https://www.sciencedirect.com/science/article/pii/S0378775315000476

[79] M. Petzl, M. Kasper, and M. A. Danzer, "Lithium plating in a commercial lithium-ion battery—A low-temperature aging study," *J. Power Sources*, vol. 275, pp. 799–807, Feb. 2015. [Online]. Available: https://www.sciencedirect.com/science/article/pii/S0378775314018928

[80] S. Schindler, M. Bauer, M. Petzl, and M. A. Danzer, "Voltage relaxation and impedance spectroscopy as in-operando methods for the detection of lithium plating on graphitic anodes in commercial lithium-ion cells," *J. Power Sources*, vol. 304, pp. 170–180, Feb. 2016. [Online]. Available: https://www.sciencedirect.com/science/article/pii/S0378775315305425

[81] Y. Chen, K.-H. Chen, A. J. Sanchez, E. Kazyak, V. Goel, Y. Gorlin, J. Christensen, K. Thornton, and N. P. Dasgupta, "Operando video microscopy of Li plating and re-intercalation on graphite anodes during fast charging," *J. Mater. Chem. A*, vol. 9, no. 41, pp. 23522–23536, 2021, doi: 10.1039/d1ta06023f.

[82] M. Petzl and M. A. Danzer, "Nondestructive detection, characterization, and quantification of lithium plating in commercial lithium-ion batteries," *J. Power Sources*, vol. 254, pp. 80–87, May 2014. [Online]. Available: https://www.sciencedirect.com/science/article/pii/S0378775313020387

[83] Q. Liu, C. Du, B. Shen, P. Zuo, X. Cheng, Y. Ma, G. Yin, and Y. Gao, "Understanding undesirable anode lithium plating issues in lithium-ion batteries," *RSC Adv.*, vol. 6, no. 91, pp. 88683–88700, 2016, doi: 10.1039/c6ra19482f.

[84] S. P. Rangarajan, Y. Barsukov, and P. P. Mukherjee, "Anode potential controlled charging prevents lithium plating," *J. Mater. Chem. A*, vol. 8, no. 26, pp. 13077–13085, 2020, doi: 10.1039/d0ta04467a.

[85] K. Xu, A. von Cresce, and U. Lee, "Differentiating contributions to 'ion transfer' barrier from interphasial resistance and Li^+ desolvation at electrolyte/graphite interface," *Langmuir*, vol. 26, no. 13, pp. 11538–11543, Jul. 2010, doi: 10.1021/la1009994.

[86] H. P. Lin, D. Chua, M. Salomon, H.-C. Shiao, M. Hendrickson, E. Plichta, and S. Slane, "Low-temperature behavior of Li-ion cells," *Electrochem. Solid-State Lett.*, vol. 4, no. 6, p. A71, Apr. 2001, doi: 10.1149/1.1368736.

[87] S. Hossain, Y.-K. Kim, Y. Saleh, and R. Loutfy, "Overcharge studies of carbon fiber composite-based lithium-ion cells," *J. Power Sources*, vol. 161, no. 1, pp. 640–647, Oct. 2006. [Online]. Available: https://www.sciencedirect.com/science/article/pii/S0378775306007804

[88] C. Sole, N. E. Drewett, and L. J. Hardwick, "Insitu Raman study of lithium-ion intercalation into microcrystalline graphite," *Faraday Discuss.*, vol. 172, pp. 223–237, Jan. 2014, doi: 10.1039/c4fd00079j.

[89] M. P. Mercer, M. Otero, M. Ferrer-Huerta, A. Sigal, D. E. Barraco, H. E. Hoster, and E. P. M. Leiva, "Transitions of lithium occupation in graphite: A physically informed model in the dilute lithium occupation limit supported by electrochemical and thermodynamic measurements," *Electrochimica Acta*, vol. 324, Nov. 2019, Art. no. 134774. [Online]. Available: https://www.sciencedirect.com/science/article/pii/S0013468619316457

[90] V. A. Sethuraman, N. Van Winkle, D. P. Abraham, A. F. Bower, and P. R. Guduru, "Real-time stress measurements in lithium-ion battery negative-electrodes," *J. Power Sources*, vol. 206, pp. 334–342, May 2012. [Online]. Available: https://www.sciencedirect.com/science/article/pii/S0378775312000730

[91] F. Schipper, E. M. Erickson, C. Erk, J.-Y. Shin, F. F. Chesneau, and D. Aurbach, "Review—Recent advances and remaining challenges for lithium ion battery cathodes," *J. Electrochem. Soc.*, vol. 164, no. 1, pp. A6220–A6228, Dec. 2016, doi: 10.1149/2.0351701jes.

[92] F. Lin, I. M. Markus, D. Nordlund, T.-C. Weng, M. D. Asta, H. L. Xin, and M. M. Doeff, "Surface reconstruction and chemical evolution of stoichiometric layered cathode materials for lithium-ion batteries," *Nature Commun.*, vol. 5, no. 1, Mar. 2014, Art. no. 3529, doi: 10.1038/ncomms4529.

[93] M. Chen, L.-L. Shao, H.-B. Yang, T.-Z. Ren, G. Du, and Z.-Y. Yuan, "Vanadium-doping of $LiFePO_4$/carbon composite cathode materials synthesized with organophosphorus source," *Electrochimica Acta*, vol. 167, pp. 278–286, Jun. 2015. [Online]. Available: https://www.sciencedirect.com/science/article/pii/S0013468615008191

[94] S. S. Zhang, "The effect of the charging protocol on the cycle life of a Li-ion battery," *J. Power Sources*, vol. 161, no. 2, pp. 1385–1391, Oct. 2006. [Online]. Available: https://www.sciencedirect.com/science/article/pii/S0378775306011839

[95] D. H. Doughty and E. P. Roth, "A general discussion of Li ion battery safety," *Electrochem. Soc. Interface*, vol. 21, no. 2, p. 37, 2012, doi: 10.1149/2.F03122if.

[96] D. R. Gallus, R. Schmitz, R. Wagner, B. Hoffmann, S. Nowak, I. Cekic-Laskovic, R. W. Schmitz, and M. Winter, "The influence of different conducting salts on the metal dissolution and capacity fading of NCM cathode material," *Electrochimica Acta*, vol. 134, pp. 393–398, Jul. 2014. [Online]. Available: https://www.sciencedirect.com/science/article/pii/S001346861400838X

[97] D. Juarez-Robles, A. A. Vyas, C. Fear, J. A. Jeevarajan, and P. P. Mukherjee, "Overdischarge and aging analytics of Li-ion cells," *J. Electrochem. Soc.*, vol. 167, no. 9, Jul. 2020, Art. no. 090558, doi: 10.1149/1945-7111/aba00a.

[98] A. J. Smith, J. C. Burns, X. Zhao, D. Xiong, and J. R. Dahn, "A high precision coulometry study of the SEI growth in Li/graphite cells," *J. Electrochem. Soc.*, vol. 158, no. 5, p. A447, Mar. 2011, doi: 10.1149/1.3557892.

[99] M. Zier, F. Scheiba, S. Oswald, J. Thomas, D. Goers, T. Scherer, M. Klose, H. Ehrenberg, and J. Eckert, "Lithium dendrite and solid electrolyte interphase investigation using OsO_4," *J. Power Sources*, vol. 266, pp. 198–207, Nov. 2014. [Online]. Available: https://www.sciencedirect.com/science/article/pii/S0378775314006351

[100] *IEEE Recommended Practice for Sizing Lead-Acid Batteries for Stationary Applications*, IEEE Standard 485-2020, 2020, pp. 1–69.

[101] W. Diao, S. Saxena, B. Han, and M. Pecht, "Algorithm to determine the knee point on capacity fade curves of lithium-ion cells," *Energies*, vol. 12, no. 15, p. 2910, Jul. 2019. [Online]. Available: https://www.mdpi.com/1996-1073/12/15/2910

[102] M. Haris, M. N. Hasan, and S. Qin, "Degradation curve prediction of lithium-ion batteries based on knee point detection algorithm and convolutional neural network," *IEEE Trans. Instrum. Meas.*, vol. 71, pp. 1–10, 2022. [Online]. Available: https://ieeexplore.ieee.org/document/9791388

[103] H. You, J. Zhu, X. Wang, B. Jiang, H. Sun, X. Liu, X. Wei, G. Han, S. Ding, H. Yu, W. Li, D. U. Sauer, and H. Dai, "Nonlinear health evaluation for lithium-ion battery within full-lifespan," *J. Energy Chem.*, vol. 72, pp. 333–341, Sep. 2022. [Online]. Available: https://www.sciencedirect.com/science/article/pii/S2095495622002030

[104] S. Tamilselvi, S. Gunasundari, N. Karuppiah, A. Razak, S. Madhusudan, V. M. Nagarajan, T. Sathish, M. Z. M. Shamim, C. A. Saleel, and A. Afzal, "A review on battery modelling techniques," *Sustainability*, vol. 13, no. 18, p. 10042, Sep. 2021. [Online]. Available: https://www.mdpi.com/2071-1050/13/18/10042

[105] J. Meng, G. Luo, M. Ricco, M. Swierczynski, D.-I. Stroe, and R. Teodorescu, "Overview of lithium-ion battery modeling methods for state-of-charge estimation in electrical vehicles," *Appl. Sci.*, vol. 8, no. 5, p. 659, Apr. 2018. [Online]. Available: https://www.mdpi.com/2076-3417/8/5/659

[106] C. Zhang, K. Li, S. Mcloone, and Z. Yang, "Battery modelling methods for electric vehicles—A review," in *Proc. Eur. Control Conf. (ECC)*, Jun. 2014, pp. 2673–2678.

[107] A. Fotouhi, D. J. Auger, K. Propp, S. Longo, and M. Wild, "A review on electric vehicle battery modelling: From lithium-ion toward lithium–sulphur," *Renew. Sustain. Energy Rev.*, vol. 56, pp. 1008–1021, Apr. 2016. [Online]. Available: https://www.sciencedirect.com/science/article/pii/S1364032115013921

[108] P. Barai, K. Smith, C.-F. Chen, G.-H. Kim, and P. P. Mukherjee, "Reduced order modeling of mechanical degradation induced performance decay in lithium-ion battery porous electrodes," *J. Electrochem. Soc.*, vol. 162, no. 9, pp. A1751–A1771, Jun. 2015, doi: 10.1149/2.0241509jes.

[109] M. Tang, S. Lu, and J. Newman, "Experimental and theoretical investigation of solid-electrolyte-interphase formation mechanisms on glassy carbon," *J. Electrochem. Soc.*, vol. 159, no. 11, pp. A1775–A1785, Aug. 2012, doi: 10.1149/2.025211jes.

[110] P. Liu, J. Wang, J. Hicks-Garner, E. Sherman, S. Soukiazian, M. Verbrugge, H. Tataria, J. Musser, and P. Finamore, "Aging mechanisms of $LiFePOs_4$ batteries deduced by electrochemical and structural analyses," *J. Electrochem. Soc.*, vol. 157, no. 4, p. A499, Mar. 2010, doi: 10.1149/1.3294790.

[111] S. Das, P. M. Attia, W. C. Chueh, and M. Z. Bazant, "Electrochemical kinetics of SEI growth on carbon black: Part II. Modeling," *J. Electrochem. Soc.*, vol. 166, no. 4, pp. E107–E118, Feb. 2019, doi: 10.1149/2.0241904jes.

[112] S. K. Madi Reddy, W. Shang, and R. E. White, "Mathematical model for SEI growth under open-circuit conditions," *J. Electrochem. Soc.*, vol. 169, no. 9, Sep. 2022, Art. no. 090505, doi: 10.1149/1945-7111/ac8ee5.

[113] R. P. Ramasamy, J.-W. Lee, and B. N. Popov, "Simulation of capacity loss in carbon electrode for lithium-ion cells during storage," *J. Power Sources*, vol. 166, no. 1, pp. 266–272, Mar. 2007. [Online]. Available: https://www.sciencedirect.com/science/article/pii/S0378775307000924

[114] M. Tang, P. Albertus, and J. Newman, "Two-dimensional modeling of lithium deposition during cell charging," *J. Electrochem. Soc.*, vol. 156, no. 5, p. A390, Mar. 2009, doi: 10.1149/1.3095513.

[115] R. D. Perkins, A. V. Randall, X. Zhang, and G. L. Plett, "Controls oriented reduced order modeling of lithium deposition on overcharge," *J. Power Sources*, vol. 209, pp. 318–325, Jul. 2012. [Online]. Available: https://www.sciencedirect.com/science/article/pii/S0378775312005423

[116] H. Ge, T. Aoki, N. Ikeda, S. Suga, T. Isobe, Z. Li, Y. Tabuchi, and J. Zhang, "Investigating lithium plating in lithium-ion batteries at low temperatures using electrochemical model with NMR assisted parameterization," *J. Electrochem. Soc.*, vol. 164, no. 6, pp. A1050–A1060, Mar. 2017, doi: 10.1149/2.0461706jes.

[117] S. Hein, T. Danner, and A. Latz, "An electrochemical model of lithium plating and stripping in lithium ion batteries," *ACS Appl. Energy Mater.*, vol. 3, no. 9, pp. 8519–8531, Sep. 2020, doi: 10.1021/acsaem.0c01155.

[118] L. Hovestadt, S. Lux, N. Koellner, A. Schloesser, and R. Hanke-Rauschenbach, "Model based investigation of lithium deposition including an optimization of fast charging lithium ion cells," *J. Electrochem. Soc.*, vol. 168, no. 5, May 2021, Art. no. 050538, doi: 10.1149/1945-7111/abfd75.

[119] T. Sun, T. Shen, Y. Zheng, D. Ren, W. Zhu, J. Li, Y. Wang, K. Kuang, X. Rui, S. Wang, L. Wang, X. Han, L. Lu, and M. Ouyang, "Modeling the inhomogeneous lithium plating in lithium-ion batteries induced by non-uniform temperature distribution," *Electrochimica Acta*, vol. 425, Sep. 2022, Art. no. 140701. [Online]. Available: https://www.sciencedirect.com/science/article/pii/S001346862200860X

[120] M. Doyle, T. F. Fuller, and J. Newman, "Modeling of galvanostatic charge and discharge of the lithium/polymer/insertion cell," *J. Electrochem. Soc.*, vol. 140, no. 6, pp. 1526–1533, Jun. 1993, doi: 10.1149/1.2221597.

[121] K. Smith and C.-Y. Wang, "Power and thermal characterization of a lithium-ion battery pack for hybrid-electric vehicles," *J. Power Sources*, vol. 160, no. 1, pp. 662–673, Sep. 2006. [Online]. Available: https://www.sciencedirect.com/science/article/pii/S0378775306001017

[122] W. B. Gu and C. Y. Wang, "Thermal-electrochemical modeling of battery systems," *J. Electrochem. Soc.*, vol. 147, no. 8, p. 2910, Aug. 2000, doi: 10.1149/1.1393625.

[123] V. Srinivasan and C. Y. Wang, "Analysis of electrochemical and thermal behavior of Li-ion cells," *J. Electrochem. Soc.*, vol. 150, no. 1, pp. A98–A106, Dec. 2002, doi: 10.1149/1.1526512.

[124] H. Ekström and G. Lindbergh, "A model for predicting capacity fade due to SEI formation in a commercial Graphite/LiFePO4Cell," *J. Electrochem. Soc.*, vol. 162, no. 6, pp. A1003–A1007, Mar. 2015, doi: 10.1149/2.0641506jes.

[125] F. M. Kindermann, J. Keil, A. Frank, and A. Jossen, "A SEI modeling approach distinguishing between capacity and power fade," *J. Electrochem. Soc.*, vol. 164, no. 12, pp. E287–E294, Aug. 2017, doi: 10.1149/2.0321712jes.

[126] C. Kupper, B. Weißhar, S. Rißmann, and W. G. Bessler, "End-of-life prediction of a lithium-ion battery cell based on mechanistic aging models of the graphite electrode," *J. Electrochem. Soc.*, vol. 165, no. 14, pp. A3468–A3480, Nov. 2018, doi: 10.1149/2.0941814jes.

[127] X.-G. Yang and C.-Y. Wang, "Understanding the trilemma of fast charging, energy density and cycle life of lithium-ion batteries," *J. Power Sources*, vol. 402, pp. 489–498, Oct. 2018. [Online]. Available: https://www.sciencedirect.com/science/article/pii/S0378775318310462

[128] K. A. Severson, P. M. Attia, N. Jin, N. Perkins, B. Jiang, Z. Yang, M. H. Chen, M. Aykol, P. K. Herring, D. Fraggedakis, M. Z. Bazant, S. J. Harris, W. C. Chueh, and R. D. Braatz, "Data-driven prediction of battery cycle life before capacity degradation," *Nature Energy*, vol. 4, no. 5, pp. 383–391, Mar. 2019, doi: 10.1038/s41560-019-0356-8.

[129] X. Wei, Z. Guo, X. Hu, C. Fang, and Y. Li, "A review of data-physical fusion methods for lithium-ion battery state estimation," in *Proc. IEEE 7th Conf. Energy Internet Energy Syst. Integr. (EI2)*, Dec. 2023, pp. 4030–4034.

[130] W. Waag, C. Fleischer, and D. U. Sauer, "Critical review of the methods for monitoring of lithium-ion batteries in electric and hybrid vehicles," *J. Power Sources*, vol. 258, pp. 321–339, Jul. 2014. [Online]. Available: https://www.sciencedirect.com/science/article/pii/S0378775314002572

[131] H. Rauf, M. Khalid, and N. Arshad, "Machine learning in state of health and remaining useful life estimation: Theoretical and technological development in battery degradation modelling," *Renew. Sustain. Energy Rev.*, vol. 156, Mar. 2022, Art. no. 111903. [Online]. Available: https://www.sciencedirect.com/science/article/pii/S1364032121011692

[132] S. Greenbank and D. Howey, "Automated feature extraction and selection for data-driven models of rapid battery capacity fade and end of life," *IEEE Trans. Ind. Informat.*, vol. 18, no. 5, pp. 2965–2973, May 2022, doi: 10.1109/TII.2021.3106593.

[133] K. Liu, X. Tang, R. Teodorescu, F. Gao, and J. Meng, "Future ageing trajectory prediction for lithium-ion battery considering the knee point effect," *IEEE Trans. Energy Convers.*, vol. 37, no. 2, pp. 1282–1291, Jun. 2022, doi: 10.1109/TEC.2021.3130600.

[134] L. Wu, X. Fu, and Y. Guan, "Review of the remaining useful life prognostics of vehicle lithium-ion batteries using data-driven methodologies," *Appl. Sci.*, vol. 6, no. 6, p. 166, May 2016. [Online]. Available: https://www.mdpi.com/2076-3417/6/6/166

[135] F. Chollet, *Deep Learning With Python*. Shelter Island, NY, USA: Manning, 2017.

[136] J. Liu, A. Saxena, K. Goebel, B. Saha, and W. Wang, "An adaptive recurrent neural network for remaining useful life prediction of lithium-ion batteries," Nat. Aeronaut. Space Admin. Moffett Field CA Ames Res., Moffett Field, CA, USA, Tech. Rep. ADA562707, 2010.

[137] A. Eddahech, O. Briat, N. Bertrand, J.-Y. Delétage, and J.-M. Vinassa, "Behavior and state-of-health monitoring of Li-ion batteries using impedance spectroscopy and recurrent neural networks," *Int. J. Electr. Power Energy Syst.*, vol. 42, no. 1, pp. 487–494, Nov. 2012. [Online]. Available: https://www.sciencedirect.com/science/article/pii/S0142061512001779

[138] Y. Zhang, R. Xiong, H. He, and M. G. Pecht, "Long short-term memory recurrent neural network for remaining useful life prediction of lithium-ion batteries," *IEEE Trans. Veh. Technol.*, vol. 67, no. 7, pp. 5695–5705, Jul. 2018, doi: 10.1109/TVT.2018.2805189.

[139] W. Li, N. Sengupta, P. Dechent, D. Howey, A. Annaswamy, and D. U. Sauer, "One-shot battery degradation trajectory prediction with deep learning," *J. Power Sources*, vol. 506, Sep. 2021, Art. no. 230024. [Online]. Available: https://www.sciencedirect.com/science/article/pii/S0378775321005528

[140] C. Strange and G. dos Reis, "Prediction of future capacity and internal resistance of Li-ion cells from one cycle of input data," *Energy AI*, vol. 5, Sep. 2021, Art. no. 100097. [Online]. Available: https://www.sciencedirect.com/science/article/pii/S2666546821000501

[141] S. Sohn, H.-E. Byun, and J. H. Lee, "Two-stage deep learning for online prediction of knee-point in Li-ion battery capacity degradation," *Appl. Energy*, vol. 328, Dec. 2022, Art. no. 120204. [Online]. Available: https://www.sciencedirect.com/science/article/pii/S0306261922014611

[142] B. Saha, K. Goebel, and J. Christophersen, "Comparison of prognostic algorithms for estimating remaining useful life of batteries," *Trans. Inst. Meas. Control*, vol. 31, nos. 3–4, pp. 293–308, Jun. 2009, doi: 10.1177/0142331208092030.

[143] A. Nuhic, T. Terzimehic, T. Soczka-Guth, M. Buchholz, and K. Dietmayer, "Health diagnosis and remaining useful life prognostics of lithium-ion batteries using data-driven methods," *J. Power Sources*, vol. 239, pp. 680–688, Oct. 2013.

[144] V. Klass, M. Behm, and G. Lindbergh, "A support vector machine-based state-of-health estimation method for lithium-ion batteries under electric vehicle operation," *J. Power Sources*, vol. 270, pp. 262–272, Dec. 2014. [Online]. Available: https://www.sciencedirect.com/science/article/pii/S0378775314011707

[145] D. Wang, Q. Miao, and M. Pecht, "Prognostics of lithium-ion batteries based on relevance vectors and a conditional three-parameter capacity degradation model," *J. Power Sources*, vol. 239, pp. 253–264, Oct. 2013. [Online]. Available: https://www.sciencedirect.com/science/article/pii/S0378775313005235

[146] D. Liu, J. Zhou, D. Pan, Y. Peng, and X. Peng, "Lithium-ion battery remaining useful life estimation with an optimized relevance vector machine algorithm with incremental learning," *Measurement*, vol. 63, pp. 143–151, Mar. 2015. [Online]. Available: https://www.sciencedirect.com/science/article/pii/S0263224114005922

[147] Y. Xiang, W. Fan, J. Zhu, X. Wei, and H. Dai, "Semi-supervised deep learning for lithium-ion battery state of health estimation using dynamic discharge profiles," *Cell Rep. Phys. Sci.*, vol. 5, Jan. 2023, Art. no. 101763.

[148] J. Yao, Z. Chang, T. Han, and J. Tian, "Semi-supervised adversarial deep learning for capacity estimation of battery energy storage systems," *Energy*, vol. 294, May 2024, Art. no. 130882.

[149] C. Bertinelli Salucci, A. Bakdi, I. K. Glad, E. Vanem, and R. De Bin, "A novel semi-supervised learning approach for state of health monitoring of maritime lithium-ion batteries," *J. Power Sources*, vol. 556, Feb. 2023, Art. no. 232429. [Online]. Available: https://www.sciencedirect.com/science/article/pii/S0378775322014069

[150] L. Ma, J. Tian, T. Zhang, Q. Guo, and C. Y. Chung, "Enhanced battery life prediction with reduced data demand via semi-supervised representation learning," *J. Energy Chem.*, vol. 101, pp. 524–534, Feb. 2025. [Online]. Available: https://www.sciencedirect.com/science/article/pii/S2095495624006910

[151] N. Guo, S. Chen, J. Tao, Y. Liu, J. Wan, and X. Li, "Semi-supervised learning for explainable few-shot battery lifetime prediction," *Joule*, vol. 8, no. 6, pp. 1820–1836, Jun. 2024. [Online]. Available: https://www.sciencedirect.com/science/article/pii/S254243512400103X

[152] M. Ye, Q. Wang, L. Yan, M. Wei, G. Lian, K. Zhao, and W. Zhu, "Enhanced robust capacity estimation of lithium-ion batteries with unlabeled dataset and semi-supervised machine learning," *Expert Syst. Appl.*, vol. 238, Mar. 2024, Art. no. 121892.

[153] C. Zhang, Y. Wang, Y. Gao, F. Wang, B. Mu, and W. Zhang, "Accelerated fading recognition for lithium-ion batteries with Nickel-Cobalt-Manganese cathode using quantile regression method," *Appl. Energy*, vol. 256, Dec. 2019, Art. no. 113841. [Online]. Available: https://www.sciencedirect.com/science/article/pii/S0306261919315284

[154] M. Aykol, C. B. Gopal, A. Anapolsky, P. K. Herring, B. van Vlijmen, M. D. Berliner, M. Z. Bazant, R. D. Braatz, W. C. Chueh, and B. D. Storey, "Perspective—Combining physics and machine learning to predict battery lifetime," *J. Electrochem. Soc.*, vol. 168, no. 3, Mar. 2021, Art. no. 030525, doi: 10.1149/1945-7111/abec55.

[155] M. Raissi, P. Perdikaris, and G. E. Karniadakis, "Physics informed deep learning (Part I): Data-driven solutions of nonlinear partial differential equations," 2017, *arXiv:1711.10561*.

[156] L. Ma, J. Tian, T. Zhang, Q. Guo, and C. Hu, "Accurate and efficient remaining useful life prediction of batteries enabled by physics-informed machine learning," *J. Energy Chem.*, vol. 91, pp. 512–521, Apr. 2024. [Online]. Available: https://www.sciencedirect.com/science/article/pii/S2095495624000214

[157] T. Hofmann, J. Hamar, M. Rogge, C. Zoerr, S. Erhard, and J. P. Schmidt, "Physics-informed neural networks for state of health estimation in lithium-ion batteries," *J. Electrochem. Soc.*, vol. 170, no. 9, Sep. 2023, Art. no. 090524.

[158] Q. Yu, Y. Nie, S. Liu, J. Li, and A. Tang, "State of health estimation method for lithium-ion batteries based on multiple dynamic operating conditions," *J. Power Sources*, vol. 582, Oct. 2023, Art. no. 233541. [Online]. Available: https://www.sciencedirect.com/science/article/pii/S0378775323009175

[159] F. Wang, Z. Zhai, Z. Zhao, Y. Di, and X. Chen, "Physics-informed neural network for lithium-ion battery degradation stable modeling and prognosis," *Nature Commun.*, vol. 15, no. 1, May 2024, Art. no. 4332.

[160] S. Zhang, Z. Liu, T. An, J. Guo, and H. Su, "An interpretable semi-supervised learning approach for battery lifespan early prognostic," in *Proc. 36th Chin. Control Decis. Conf. (CCDC)*, May 2024, pp. 7–14.

[161] J. Tian, R. Xiong, W. Shen, and F. Sun, "Electrode ageing estimation and open circuit voltage reconstruction for lithium ion batteries," *Energy Storage Mater.*, vol. 37, pp. 283–295, May 2021. [Online]. Available: https://www.sciencedirect.com/science/article/pii/S2405829721000611

[162] X. Liu, H. Peng, B. Li, X. Chen, Z. Li, J. Huang, and Q. Zhang, "Untangling degradation chemistries of lithium–sulfur batteries through interpretable hybrid machine learning," *Angew. Chem.*, vol. 134, no. 48, Nov. 2022, Art. no. e202214037.
[163] M. Raissi, P. Perdikaris, and G. Em Karniadakis, "Physics informed deep learning (Part II): Data-driven discovery of nonlinear partial differential equations," 2017, *arXiv:1711.10566*.
[164] F. von Bulow and T. Meisen, "State of health forecasting of heterogeneous lithium-ion battery types and operation enabled by transfer learning," in *Proc. PHM Soc. Eur. Conf.*, vol. 7, Jun. 2022, pp. 490–508.
[165] W. Guo, Z. Sun, S. B. Vilsen, J. Meng, and D. I. Stroe, "Review of 'grey box' lifetime modeling for lithium-ion battery: Combining physics and data-driven methods," *J. Energy Storage*, vol. 56, Jan. 2022, Art. no. 105992. [Online]. Available: https://www.sciencedirect.com/science/article/pii/S2352152X22019806

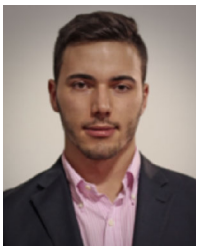

PEDRO LOZANO RUIZ (Student Member, IEEE) received the B.Sc. degree in energy engineering from the University of Seville, in 2017, and the M.Sc. degree in sustainable energy technology from Delft University of Technology, in 2024. He is currently a Battery Engineer with Sonova AG, specializing in li-ion battery charging optimization, performance, and degradation modeling.

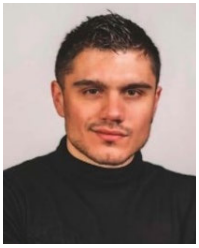

NIKOLAOS DAMIANAKIS (Graduate Student Member, IEEE) received the joint B.Sc. and M.Sc. degrees in electrical engineering from the National Technical University of Athens, in 2018, and the M.Sc. degree in electrical power engineering from the Technical University of Delft, in 2021, where he is currently pursuing the Ph.D. degree in coordinated power control of smart loads & energy storage systems in DC power grids with the DC Systems, Energy Conversion, and Storage Group, Electrical Sustainable Energy Department.

GAUTHAM RAM CHANDRA MOULI (Member, IEEE) received the bachelor's degree in electrical engineering from the National Institute of Technology Trichy, India, in 2011, the master's degree from Delft University of Technology, in 2013, and the Ph.D. degree from Delft University, in 2018, for the development of a solar-powered V2G electric vehicle charger with smart charging, compatible with CHAdeMO and CCS/COMBO. He is currently an Assistant Professor in electric mobility with the DC Systems, Energy Conversion, and Storage Group, Department of Electrical Sustainable Energy, Delft University of Technology. His current research interests include electric vehicles, EV charging, batteries, power electronics, and grid integration.